NAVAL
POSTGRADUATE
SCHOOL

MONTEREY, CALIFORNIA

THESIS

RADAR ABSORBING MATERIAL DESIGN

by

Cihangir Kemal Yuzcelik

September 2003

Thesis Advisor:	David Jenn
Second Reader:	Richard Adler

Approved for public release, distribution is unlimited

THIS PAGE INTENTIONALLY LEFT BLANK

REPORT DOCUMENTATION PAGE			Form Approved OMB No. 0704-0188
Public reporting burden for this collection of information is estimated to average 1 hour per response, including the time for reviewing instruction, searching existing data sources, gathering and maintaining the data needed, and completing and reviewing the collection of information. Send comments regarding this burden estimate or any other aspect of this collection of information, including suggestions for reducing this burden, to Washington headquarters Services, Directorate for Information Operations and Reports, 1215 Jefferson Davis Highway, Suite 1204, Arlington, VA 22202-4302, and to the Office of Management and Budget, Paperwork Reduction Project (0704-0188) Washington DC 20503.			
1. AGENCY USE ONLY *(Leave blank)*	**2. REPORT DATE** September 2003	**3. REPORT TYPE AND DATES COVERED** Master's Thesis	
4. TITLE AND SUBTITLE: Title (Mix case letters) Radar Absorbing Material Design			**5. FUNDING NUMBERS**
6. AUTHOR(S)			
7. PERFORMING ORGANIZATION NAME(S) AND ADDRESS(ES) Naval Postgraduate School Monterey, CA 93943-5000			**8. PERFORMING ORGANIZATION REPORT NUMBER**
9. SPONSORING /MONITORING AGENCY NAME(S) AND ADDRESS(ES) N/A			**10. SPONSORING/MONITORING AGENCY REPORT NUMBER**
11. SUPPLEMENTARY NOTES The views expressed in this thesis are those of the author and do not reflect the official policy or position of the Department of Defense or the U.S. Government.			
12a. DISTRIBUTION / AVAILABILITY STATEMENT Approved for public release, distribution is unlimited			**12b. DISTRIBUTION CODE**

13. ABSTRACT ***(maximum 200 words)***

Low observable platforms have extremely low radar cross section specifications that cannot be achieved by shaping alone. The application of radar absorbing material is necessary, in which case the appropriate constitutive parameters and thickness must be selected. The universal design chart gives combinations of μ, ε and t that provide zero specular reflection at normal incidence. Three different backing materials were used to generate the charts: (1) perfect electric conductor, (2) free space, and (3) graphite. One can pick the required values from the charts for an ideal zero reflection dielectric/magnetic layer. The extension to other materials is straightforward. Numerical simulations of coated plates were performed to estimate the effectiveness of the absorbing layers in reducing radar cross section. The reduction in monostatic radar cross section value is shown by plotting the radar cross section of the plate with and without radar absorbing material.

14. SUBJECT TERMS Radar cross section reduction techniques, Radar absorbing materials, Matched surface RAM, Universal design charts			**15. NUMBER OF PAGES** 83
			16. PRICE CODE
17. SECURITY CLASSIFICATION OF REPORT Unclassified	**18. SECURITY CLASSIFICATION OF THIS PAGE** Unclassified	**19. SECURITY CLASSIFICATION OF ABSTRACT** Unclassified	**20. LIMITATION OF ABSTRACT** UL

NSN 7540-01-280-5500 Standard Form 298 (Rev. 2-89)
Prescribed by ANSI Std. 239-18

THIS PAGE INTENTIONALLY LEFT BLANK

Approved for public release, distribution is unlimited

RADAR ABSORBING MATERIAL DESIGN

Cihangir Kemal Yuzcelik
1st Lieutenant., Turkish Air Force
Industrial Engineering, Turkish Air Force Academy, 1997

Submitted in partial fulfillment of the
requirements for the degree of

MASTER OF SCIENCE IN SYSTEMS ENGINEERING

from the

NAVAL POSTGRADUATE SCHOOL
September 2003

Author: Cihangir Kemal Yuzcelik

Approved by: David Jenn
Thesis Advisor

Richard Adler
Second Reader

Dan Boger
Chairman, Department of Information Sciences

THIS PAGE INTENTIONALLY LEFT BLANK

ABSTRACT

Low observable platforms have extremely low radar cross section specifications that cannot be achieved by shaping alone. The application of radar absorbing material is necessary, in which case the appropriate constitutive parameters and thickness must be selected. The universal design chart gives combinations of μ, ε and t that provide zero specular reflection at normal incidence. Three different backing materials were used to generate the charts: (1) perfect electric conductor, (2) free space, and (3) graphite. One can pick the required values from the charts for an ideal zero reflection dielectric/magnetic layer. The extension to other materials is straightforward. Numerical simulations of coated plates were performed to estimate the effectiveness of the absorbing layers in reducing radar cross section. The reduction in monostatic radar cross section value is shown by plotting the radar cross section of the plate with and without radar absorbing material.

THIS PAGE INTENTIONALLY LEFT BLANK

TABLE OF CONTENTS

LIST OF FIGURES

THIS PAGE INTENTIONALLY LEFT BLANK

LIST OF TABLES

THIS PAGE INTENTIONALLY LEFT BLANK

ACKNOWLEDGMENTS

I would like to thank to my beloved country, Turkey (Turkiye), Turkish Nation and Turkish Air Force who brought me up as an officer, a fighter pilot and BS and MS degrees in academic fields.

I would like to express my most sincere gratitude to Professor David Jenn, Naval Postgraduate School, Monterey, CA for his precious contributions, guidance and reference in the completion of this work. He always assisted me with patience and answered my questions patiently and repeatedly whenever or wherever I stopped him. I really appreciate him and take him as an admirable example for my academic career. I would also like to thank to Professor Richard Adler for agreeing to be the second reader to the thesis. Both of them prepared me in electromagnetism, antenna theory, radar and radar cross section theory that formed a basis to my thesis work.

I would like to thank to my mother, Fahriye Yuzcelik, my father, Izzettin Yuzcelik and my sister, Ceyda Yuzcelik for their endless love, support and understanding. You are the wind beneath my wings!

I would like to thank to my friends back in Turkey and in Naval Postgraduate School for their support and help, for sharing my sorrows and happiness, for feeding me repeatedly, for cheering me up, thanks for everything.

Finally, I would like to dedicate this work to the Turkish soldiers and M. Kemal Ataturk, who has been protecting our independence and freedom for thousands years, for our glorious history and future.

THIS PAGE INTENTIONALLY LEFT BLANK

I. INTRODUCTION

A. BACKGROUND

In today's military aviation, in the art of dogfighting, the primary objective is to detect threats as early as possible in order to employ weapons effectively and to be undetectable to increase survivability. The famous motto in the fighter pilot's world is "to stay alive, hide yourself and see your opponent before he sees you." One side of the battle is the high technology airborne radars; the other side is radar cross section reduction techniques.

The two most often employed radar cross section reduction (RCSR) techniques are shaping and use of radar absorbing materials for radar cross section reduction. In current radar cross section (RCS) designs, shaping techniques are considered the first step of RCS control. The objective of shaping is to design the platform's surfaces and the edges to reflect or diffract the incident wave in directions away form the radar, and is primarily applied to establish a low RCS in the main threat sectors. However the modification of an aircraft's shape is limited to certain aerodynamic principles and within last three decades, the shaping technique has been applied excessively in the design of fighter aircraft such as the F-117. Recent design approaches generally opt for a balance between shaping and other reduction techniques. Therefore, radar absorbing material (RAM) engineering has become an important area of research.

Radar absorbing materials reduce the energy reflected back to the radar by means of absorption. The technique is based on an arrangement of dielectric or magnetic materials that present the appropriate impedance to the incident wave. The general idea is to establish an impedance at the RAM surface that poses good matching and absorbing qualities, so that it can attenuate the radar wave once it enters the material.

The use of radar absorbing material is one aspect of a comprehensive platform design approach. It is a trade-off in which advantages are balanced against disadvantages, and the systems engineering approach is applied. The use of radar absorbing materials enables remarkable reduction in the platform's radar cross section. On the other hand, it has disadvantages like added weight, cost, and the requirement of high maintenance.

In this study, the theory underlying radar absorbing material techniques is summarized, with emphasis given to the matched surface impedance technique. This technique employs combination of dielectric and magnetic materials to form an absorbing layer that results in zero reflection over a specific range of wavelengths.

B. OBJECTIVES

The objective of this thesis is to summarize RCS, to analyze the theory related to the matched surface RAM technique, and to generate universal design charts based on matched surface RAM theory for specular absorbers. Numerical simulations of coated plates are used to estimate the effectiveness of the layers in reducing RCS, and examine the sensitivity of performance to small changes to the layer's constituent parameters.

C. ORGANIZATION OF THESIS

In Chapter II, the methods of controlling radar cross section and penalties of implementing these methods are discussed. The four basic techniques for reducing radar cross section (target shaping, radar absorbing materials, passive cancellation, and active cancellation) are summarized with their advantages and disadvantages. The two most often employed methods, shaping and the use of radar absorbing materials, are examined in detail.

In Chapter III, the basic theorems and theory underlying the use of radar absorbing materials for RCS reduction are described, including the electronic loss mechanisms. RAM design methods, the types of RAM structures, and various implementations are discussed.

In Chapter IV, the analysis of matched surface RAM and zero specular reflection absorbers are discussed. The equations related to specular absorbers are analyzed based on the transmission line approach. Numerical methods for solving the transcendental equations, and presentation of the results in the form of a universal design chart for zero specular reflection are given.

In Chapter V, the results of the Microwave Studio simulations of coated plates are shown. The radar absorbing materials are selected based on universal design charts generated in Chapter IV.

In Chapter VI, conclusions and suggestions for future studies are discussed.

THIS PAGE INTENTIONALLY LEFT BLANK

II. RADAR CROSS SECTION REDUCTION (RCSR) TECHNIQUES

A. INTRODUCTION

This chapter evaluates methods of controlling RCS and the penalties in implementing these methods. There are four basic techniques for reducing radar cross section: (1) target shaping, (2) radar absorbing materials, (3) passive cancellation, and (4) active cancellation.

Radar cross section reduction (RCSR) is a trade-off study in which the systems engineering approach is applied, and advantages are balanced against disadvantages. For example, the modification of an aircraft's shape is limited to certain aerodynamic principles. If radar absorbing materials (RAM) are used, monostatic radar cross section reduction is obtained by the absorption of energy within the RAM, thus leaving the RCS levels relatively unchanged in other directions. On the other hand, the use of RAM has disadvantages like added weight, cost, and the requirement of high maintenance.

Reduction methods are generally limited to a small spatial region. The platform design process must address how much RCS reduction is required based on the platform's mission, and the additional cost of manufacturing and maintenance.

B. THE FOUR BASIC TECHNIQUES OF RCSR

The following sections provide a summary of each RCSR technique. The two most often applied ones, shaping and radar absorbing materials techniques, are examined first. In current RCS designs, shaping techniques are primarily applied to establish a low RCS in the main threat sections. Radar absorbing materials are then used to reduce the effects of the creeping waves or traveling waves, or where shaping is not sufficient.

1. Shaping

Traditionally, shaping is considered the first step of RCS control. The objective of shaping is to design the platform's surfaces and edges to reflect or diffract the incident RF wave in directions away form the radar. This cannot be accomplished for all aspect angles, within the entire sphere of solid angles, because there will always be viewing

angles at which surfaces are seen at normal incidence, and at these angles the echoes will be high. The success of shaping depends on the existence of angular sectors over which low radar cross section is less important than others. Shaping is a high-frequency technique based on geometrical optics; it is implicit in this method that the target is very large electrically [1].

It is usually best to keep large surfaces as flat and smooth as possible so that the specular flash is confined to a very narrow angular region. The larger the area, the higher the maximum RCS, and the faster it drops off [2]. For an aircraft the forward cone of angles is the primary interest for RCSR. Hence, shifting the large cross sections out of the forward sector toward broadside is desired. The forward section includes the elevation plane as well as the azimuth plane. If a target is hardly ever seen from above, echo sources, such as engine intakes, can be placed on the top side of the target where they may be hidden by the forward portion of the body when viewed from below. Similarly, for a low flyer such as a strike aircraft, whose major threats might be look-down radars, engine inlets might instead be placed on the underside of the fuselage [1].

The Lockheed F-117A (Figure 1) is an example of heavily applied surface faceting. Edges are parallel so that the majority of the edge effects are collectively directed away from important viewing angles. The Northrop B-2 also uses some faceting, especially on the trailing edges of the wing. In planform (Figure 2), the straight edges are dominant [2].

For more “boxy” structures such as ships and ground vehicles, dihedral and trihedral corners, and “top hats” (right circular cylinders with axes perpendicular to a flat plane) are the major RCS contributors. They can be avoided by bringing intersecting surfaces together at acute or obtuse angles. Because of the presence of the sea surface, vertical bulkheads and masts on ships, in particular, form efficient corners, and the effect can be reduced by tilting the bulkheads away from the vertical. However, this virtually impossible to do with existing vessels and therefore is a real consideration only in new designs. Even in the case of a new design, the amount of bulkhead tilt is a trade-off between RCSR performance and cost [1].

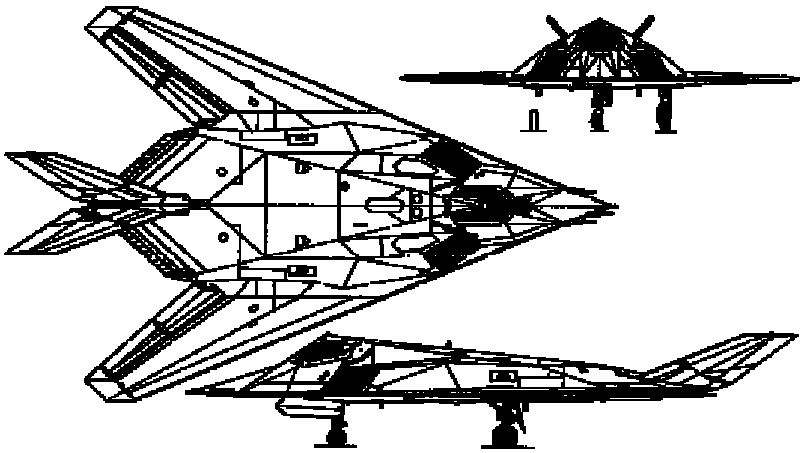

Figure 1. Planform of the Lockheed F-117 (After[3]).

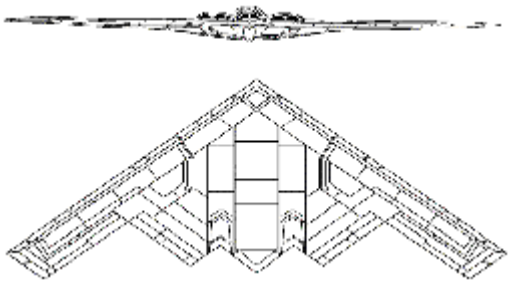

Figure 2. Planform of the Northrop B-2 (After[3]).

2. Radar Absorbing Materials

The radar absorbing materials reduce the energy reflected back to the radar by means of absorption. Radar energy is absorbed through one or more of several mechanisms, which may involve the dielectric or magnetic properties of the materials. The loss is actually the conversion of radio frequency energy into heat, and although most absorbers do not dissipate enough energy to become even detectably warm when illuminated by a radar, this is nevertheless the mechanism by which they operate.

Underlying the operation of RAM is the fact that substances either exist or can be fabricated whose indices of refraction are complex numbers. In the index of refraction, which includes magnetic as well as electric effects, the imaginary part accounts for loss. At microwave frequencies, the loss is due to the finite conductivity of the material, as well as energy expended by molecules in attempting to follow the oscillating fields of an impressed wave. It is customary to lump the effects of all loss mechanisms into the permittivity and permeability of the material, both of which can be complex [1].

In summary, the requirements of a RAM for use in RCS reduction are: (1) the absorbing material should have adequate frequency response, (2) it should work for two orthogonal polarizations, and (3) it should work with the specified aspect angle characteristics [4]. To choose a RAM that simultaneously satisfies all of these requirements, and yet is physically realizable is difficult, if not impossible. Considerations of weight and environment (e.g., temperature, rain, snow, etc.) play an important role in deciding the thickness of any RAM coating.

The theory and analysis of RAM will be discussed further in Chapter III.

3. Passive Cancellation

Passive cancellation refers to RCS reduction by introducing a secondary scatterer to cancel with the reflection of the primary target. This method is also known as impedance loading.

The basic concept is to introduce an echo source whose amplitude and phase can be adjusted to cancel another echo source. This can be accomplished for relatively simple objects, provided that a loading point can be identified on the body. A port can be

machined in that body, and the size and the shape of the interior cavity can be designed to present optimum impedance at the aperture. Unfortunately, even for simple bodies, it is extremely difficult to generate the required frequency dependence for this built-in impedance, and the reduction obtained for one frequency rapidly disappears as the frequency changes [1].

In addition to this, typical weapons platforms are hundreds of wavelengths in size and have dozens, if not hundreds of echo sources. Clearly, it is not practical to devise a passive cancellation treatment for each of these sources. Even when cancellation is introduced at one frequency, the cancellation can revert to reinforcement with a small change in frequency or viewing angle. It is evident that a fair amount of information about the threat and the target itself is required: the threat radar frequency, direction, and polarization, and the target RCS in the direction of the threat [1]. Note that there is a gray area between the technologies of absorbing materials and passive cancellation. For example, a layer of lossy dielectric coating applied to a target could fall into either category.

4. Active Cancellation

Active cancellation involves the process of modifying and retransmitting the received radar signal. The target must emit radiation in the same time with the received pulse whose amplitude and phase cancel the reflected energy. The required data are the angle of arrival, intensity, waveform and frequency of the received wave. An active cancellation system should sense these data accurately and then reradiate the pulse with proper amplitude and phase. Obviously, this requires a challenging task for the system, as the frequency increases the work becomes much more difficult.

There are two levels of cancellation:

1. Fully active: The cancellation network receives, amplifies, and retransmits the threat signal such that it is out of phase with the static RCS of the target. The transmitted signal amplitude, phase, frequency and polarization can be adjusted to compensate for changing threat parameters.

2. Semiactive: No boost in threat signal energy is provided by the cancellation network, but passive adjustable devices in the network allow the reradiated signal to compensate for limited changes in the threat signal parameters [2].

The demands for a fully active system are almost always so severe as to make it impractical. It requires a transmitter and antennas that cover the anticipated threat angles, frequencies, incident power densities, and polarization. Knowledge of the threat direction is required, as well as the target's own RCS. A semiactive system is not as complicated in terms of hardware, but the use of adjustable devices still requires bias lines, controller units, and a computer with the appropriate data bases [2].

C. THE PENALTIES OF RCSR

Each of the described techniques of RCSR brings up its own disadvantages along with its advantages and therefore requires trade-offs. The entire systems engineering approach is required to evaluate the final system design.

The first and unavoidable penalty of RCSR is the additional cost. The others are: reduced payload, added weight, required high maintenance, and reduced range or other operational limitations. The mission of the platform and the severity of the threat environment will determine the required RCSR and drive the trade-off study.

RCSR is just one aspect of the entire platform design which is affected by other sensors and signatures (infrared, acoustic, visual, etc.). An optimum design must be devised in order to maximize the objectives of the platform.

D. SUMMARY

In this chapter the four basic RCSR techniques were presented. Of the four, the use of shaping and radar absorbing material design are the most used to date.

Shaping is considered the first step of RCS control, and it is broadband as long as the wavelength is short compared to the platform dimensions (i.e., the "high frequency" regime). The objective of shaping is to orient the target surfaces and the edges to deflect the scattered energy in directions away form the radar.

Radar absorbing materials strive is to reduce the energy reflected back to the radar by means of absorption or destructive interference. Radar energy is absorbed through one or more of several mechanisms, which may involve the dielectric or magnetic properties of the materials.

In designing a RAM it is necessary to choose the dielectric and magnetic properties and thickness to minimize the reflection over the maximum possible frequency range. This problem is addressed in Chapter III.

THIS PAGE INTENTIONALLY LEFT BLANK

III. RADAR ABSORBING MATERIALS

A. INTRODUCTION

In addition to shaping an object to obtain a low radar cross section over a specified range of aspect angles, the application of radar absorbing materials may further reduce the radar cross section over a specified range of both frequencies and aspect angles. Therefore the study of radar absorbing materials is crucial in order to minimize the cross section of an object.

The technique is based on finding an arrangement of dielectric or magnetic materials that can present the appropriate impedance to the incident wave. The general idea is to establish a desirable impedance which poses good matching and absorbing qualities, so that the RAM can accept and then attenuate the incident wave.

In this chapter, the basic theory underlying absorbers is first illustrated, and then the electronic loss mechanisms are presented. In the following parts, the design methods, the types of current RAM structures, and various implementations are discussed.

B. ELECTROMAGNETIC LOSS MECHANISMS

At radar frequencies a reduction in reflection from an object can be achieved by one of two mechanisms: (1) absorption, and (2) cancellation. Coatings, also referred as resonant absorbers, reduce RCS by the cancellation of multiple reflections. Absorption is transfer of incident wave's energy to the material. The primary property of a radar absorbing material is to dissipate the energy of the incident wave into heat. These materials have constitutive parameters that are complex numbers.

The loss mechanisms are accounted for in the permittivity (ε) and permeability (μ) of the material. When expressing complex permittivity and permeability, the relative permittivity (ε_r) and the relative permeability (μ_r) which are normalized by the free space values ε_0, μ_0 are used.

The complex notation for ε_r and μ_r is normally given as

$$\varepsilon = \varepsilon' - j\varepsilon'' = \varepsilon_0(\varepsilon_r' - j\varepsilon_r''),$$
$$\mu = \mu' - j\mu'' = \mu_0(\mu_r' - j\mu_r''), \tag{3.3}$$

where the real part (energy storage part) is shown as a prime, and the imaginary part (loss part) is shown as a double prime.

At microwave frequencies the absorbed energy can be transferred to the molecules, similar to ohmic loss for conductors. As the wave energy is transferred to the material the molecular dipoles oscillate. The loss amount is determined by the imaginary parts of permeability and permittivity or, equivalently, the loss tangents,

$$\tan\delta_\varepsilon = \varepsilon''/\varepsilon',$$
$$\tan\delta_\mu = \mu''/\mu'. \tag{3.4}$$

They are called loss tangents because they are a measure of loss in the medium. The loss tangents are typically in the range of 0.001-0.1 and therefore the attenuation of the wave in decibels per meter is quite small. In the general case, the majority of loss for an electric absorber is due to the finite conductivity of material. On the other hand, the loss for magnetic absorbers is due to magnetization at microwave frequencies. Frequently it is convenient to express the loss in terms of conductivity

$$\varepsilon_r'' = \sigma / \omega\varepsilon_0 \tag{3.5}$$

where σ is conductivity and ω is radian frequency. In polar notation, the relative values are defined as

$$\varepsilon_r = |\varepsilon_r| e^{j\delta_\varepsilon}$$
$$\mu_r = |\mu_r| e^{j\delta_\mu} \tag{3.6}$$

The phase velocity in the medium is

$$u_p = \frac{\omega}{\beta} = \frac{c}{\sqrt{\mu_r'\varepsilon_r'}}. \tag{3.7}$$

Similarly, the intrinsic impedance is expressed in terms of μ_r and ε_r as,

$$\eta = \eta_0 \sqrt{\mu_r \varepsilon_r} \tag{3.8}$$

where η_0 is the intrinsic impedance of free space, and equal to 120π or approximately $377\,\Omega$.

In practical applications, a layer of dielectric will often be backed by a conducting surface. In that case, a transmission line analysis can be performed to find the effective input impedance at the front face of the layer [1]. For a flat metallic surface coated with a thin layer of dielectric material (frequently called a Dallenbach layer), the characteristic input impedance Z_{in} is given by,

$$Z_{in} = \sqrt{\mu_r / \varepsilon_r}\, \tanh(-jk_o t\sqrt{\mu_r \varepsilon_r}) \tag{3.9}$$

where t is the thickness of the layer as shown in Figure 3. In the transmission line equivalent, the reflection coefficient is defined as

$$\Gamma = \frac{Z_{in} - Z_0}{Z_{in} + Z_0}, \tag{3.10}$$

where it can be expressed as

$$\Gamma = \frac{Z_{in}/Z_0 - 1}{Z_{in}/Z_0 + 1}. \tag{3.11}$$

It is clear from Equations (3.10) and (3.11) that if $\Gamma = 0$ then $Z_{in} = Z_0$ and the load is said to be matched to the line. Thus, there will be no reflected wave at the outer face.

The objective of RAM design is to obtain a material for which the reflection coefficient is as small as possible over as wide a frequency range as possible. It is clear that unless the material has some loss, the amplitude of the reflection coefficient will be controlled entirely by the phase and amplitude relationship between the portion of the incident wave reflected at the front surface and the portion returning by reflections at the backing surface [1].

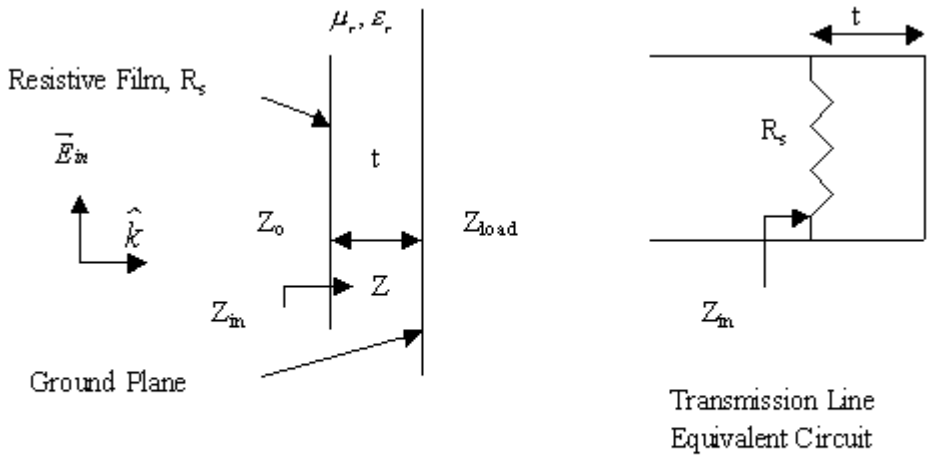

Figure 3. Specular Reflection Schematic (After [2])

C. THEOREMS FOR ABSORBERS

Weston [5] developed two theorems for backscattering from absorber coated conducting bodies that are illuminated by plane waves.

Theorem 1: If a target has equal values for relative permittivity and permeability, that is, $\varepsilon / \varepsilon_0 = \mu / \mu_0$ at each point, then the backscattered field is zero, if the shape and material of the body remain unchanged for a 90 degree rotation of the body around the direction of incidence, which is also the direction of observation.

A wave incident along the axis of symmetry of a body of revolution satisfies the geometric requirements of the theorem. If the body has constant permeability and permittivity, they must be equal: $\mu_r = \varepsilon_r$ [2].

Theorem 2: For a plane wave incident on a target, the backscattered fields will be zero if the shape and constituent parameters of the target are invariant with respect to a 90 degree rotation around the direction of incidence (observation), and if the intrinsic impedance of the material is equal to the impedance of free space, $\eta = \eta_0$, and the following impedance boundary condition is satisfied on the surface of the body [4]:

$$\vec{E} = (\hat{n} \bullet \vec{E})\hat{n} = \eta(\hat{n} \times \vec{H}) \tag{3.1}$$

where $\hat{n}$ is the unit outward normal to the surface and $\vec{E}$ and $\vec{H}$ are the electric and magnetic fields of the incident plane wave,

$$\eta = \sqrt{\frac{\mu}{\varepsilon}} = \eta_0 \sqrt{\frac{\mu_r}{\varepsilon_r}},$$
$$\eta_0 = \sqrt{\frac{\mu_0}{\varepsilon_0}}. \tag{3.2}$$

These theorems are derived directly from the Maxwell's equations and the boundary conditions which apply to any frequency and include all possible scattering and loss mechanisms. Unfortunately, practical radar targets do not satisfy the geometry limitations imposed by the theorems. However, the condition that $\mu_r = \varepsilon_r$ does shed some insight into the reduction problem. Because the impedance of a medium relative free space is essentially determined by $\sqrt{\mu_r / \varepsilon_r}$, equal permeability and permittivity yield an impedance in the medium Z_0. Consequently, the reflection coefficient between the free space and the medium is zero. Note that this applies only to the specular field. Diffractions from the edges and surface waves could still yield a nonzero scattered field for a finite interface. The nonspecular contributions to scattering will be zero only if the above- mentioned geometrical conditions are satisfied [2].

D. DIELECTRIC MULTILAYER ABSORBER DESIGN AND PERFORMANCE

The objective in the design of radar absorbing material is to obtain a layer (or layers) of the least thickness, having the lowest reflection coefficient, operating within a wide frequency range, easily applied, low-cost, light weight and long-lasting.

In the following sections the RAM types that are commonly used are depicted based on their design characteristics and performance. The descriptions start with

Salisbury screens and Dallenbach layers which are the two oldest and most basic types of absorbers. Then the discussion is extended to broadband absorbers.

1. Salisbury Screens and Dallenbach Layers

The Salisbury screen (Figure 4) is formed by placing a resistive sheet above the object's surface in order to create a resonant absorber. If the resistive film is $\lambda/4$ from the conductor, then a quarter-wavelength transmission line section transforms the short circuit at the conductor plate into an open circuit (conductance, G=0). Thus,

$$\frac{1}{Z_{in}} = \frac{1}{R_s} + \frac{1}{\infty} = \frac{1}{R_s}. \tag{3.12}$$

The reflection coefficient will be zero when $R_s = 377\Omega$. Recall that, when the line is quarter-wave length or $\lambda/4 + n\lambda/2$, where n=0 or a positive integer, a matched load is provided and no reflection occurs. Therefore, the Salisbury screen is most effective at normal incidence.

For oblique incidence of a plane wave onto the absorber, the magnitude of the reflection coefficients for parallel and perpendicular polarizations are expressed in terms of θ

$$\left|\Gamma_{\perp}\right| = \left|\Gamma_{\parallel}\right| \simeq \frac{1-\cos\theta}{1+\cos\theta}. \tag{3.13}$$

In Figure 5, Equation (3.13) is plotted or angles up to 35^{o}, where θ is the angle off-normal. Where the reflection coefficient is smaller than 0.1, the performance is better than 20 dB.

For other values of resistivity or spacing, the cancellation is not complete. Neither is it complete for a finite screen size, even for ideal materials, because of edge diffractions from the screen and ground plane [2]. Rapid oscillations for large spacings render the absorber ineffective over a wide frequency range [1].

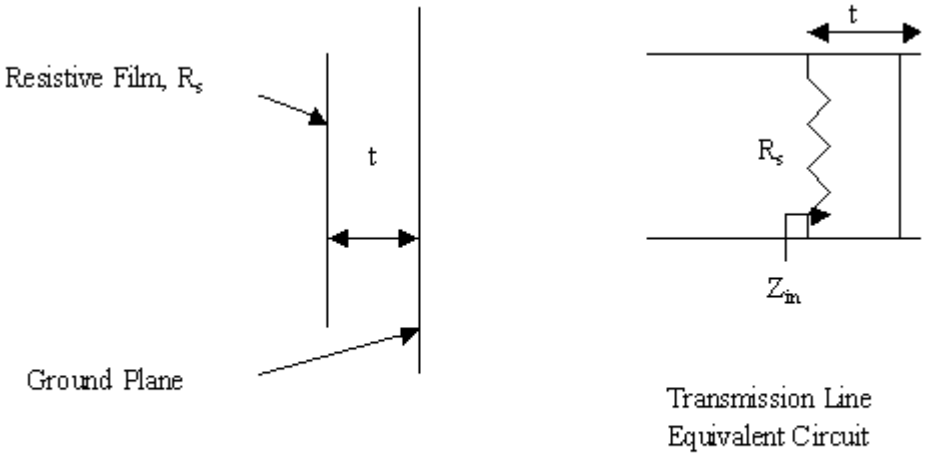

Figure 4. Salisbury Screen (After [2])

The Dallenbach layer (Figure 6) consists of a homogeneous lossy layer backed by a metal plate. Similar to the Salisbury screen, the reflection from the outer surface cancels the reflection from the back surface. From Equation (3.10), the reflection coefficient at the outer surface is

$$\Gamma = \frac{Z_{in} - Z_o}{Z_{in} + Z_o}$$

where

$$Z_{in} = Z_1 \frac{Z_{load} + jZ_1 \tanh(\gamma t)}{Z_1 + jZ_{load} \tanh(\gamma t)} \tag{3.14}$$

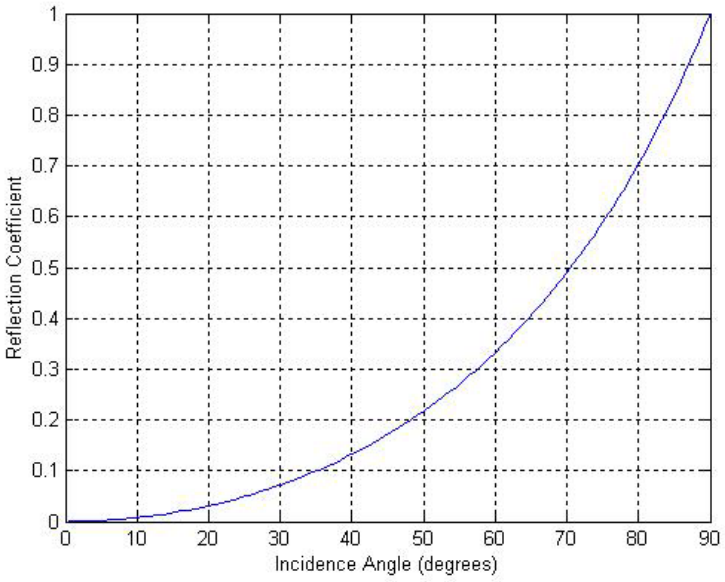

Figure 5. Reflection coefficient as a function of angle of incidence

Z_1 is the impedance of the layer material, Z_{load} is the impedance of the back material and t is thickness of the outer surface. The impedance Z_1 can be written as

$$Z_1 = \sqrt{\mu/\varepsilon} = \sqrt{\frac{\mu' - j\mu''}{\varepsilon' - j\varepsilon''}}. \tag{3.15}$$

The complex propagation constant is

$$\gamma = j\omega\sqrt{\mu\varepsilon}. \tag{3.16}$$

As it is clearly seen, the reflection at the surface of a material is due to the impedance change seen by the wave at the interface between the two media. Therefore, if a material can be found whose impedance relative to the free space equals 1 (i.e., $\mu_r = \varepsilon_r$), there will be no reflection at the surface. In this case the attenuation will depend on the loss properties of the material $(\varepsilon_r'', \mu_r'')$ and electrical thickness. Unfortunately, materials with the appropriate dielectric and magnetic properties to act as a matched RAM over any frequency bandwidth are difficult to find. So the objective is to optimize the loss at the given frequency with available material.

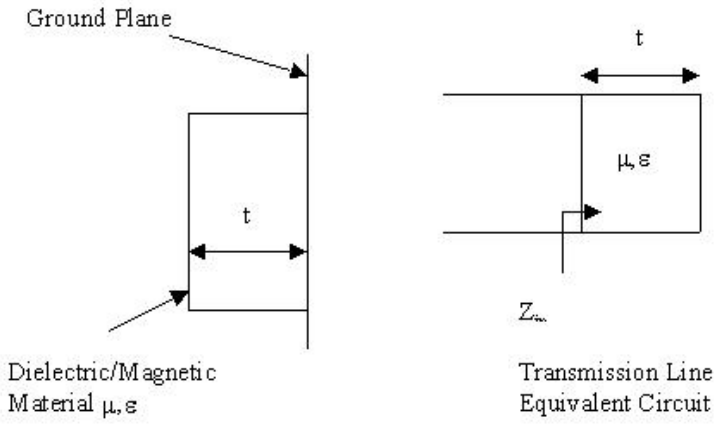

Figure 6. Dallenbach Layer (After [2])

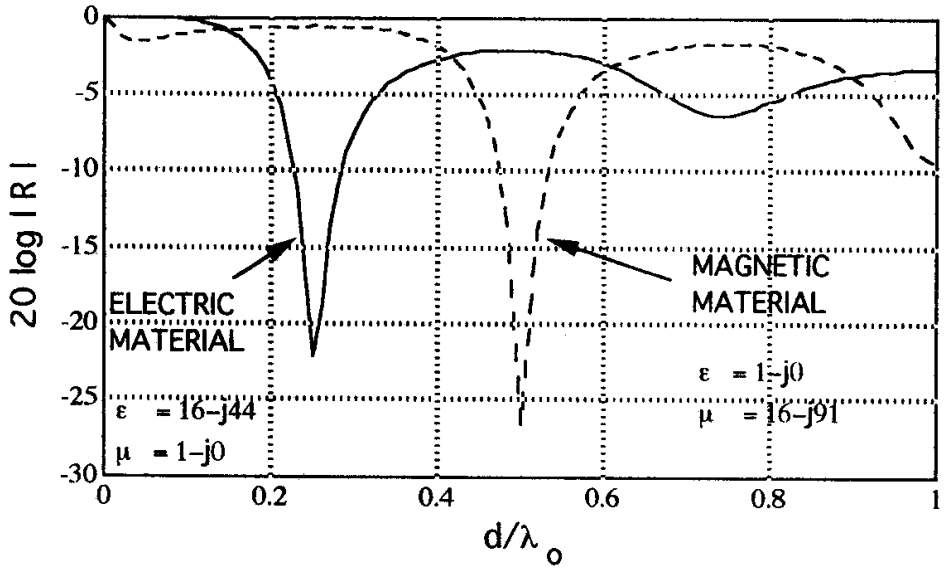

Figure 7. Performance of Dallenbach Layers (From [2]).

Figure 7 shows the reflection coefficient of Dallenbach layers as a function of thickness for various values of permeability and permittivity. The best RCSR performance for nonmagnetic materials occurs at quarterwave length ($0.25\lambda_0$, λ_0 is the

free space wavelength) where $\mu_r = 1, \varepsilon_r > 1$ and second resonance occurs at $0.50\lambda_o$ where $\varepsilon_r = 1, \mu_r > 1$ for magnetic materials.

2. Multilayer Dielectric Absorbers

One objective of RAM design is to have the radar absorbing material efficient over a wide range of frequencies. However, by using a single-layer absorber the bandwidth obtained is generally insufficient. The multilayer dielectric absorber concept benefits from the change of effective impedance with the distance into the material, so that the reflections are minimized. Two important multilayer dielectric absorbers will be discussed in this section: (1) Jaumann absorbers, and (2) graded dielectric absorbers.

Jaumann absorbers are formed by positioning the multilayer resistive sheets from the sheet with the highest resistivity in the front and the lowest one at the back, so that the bandwidth of a Salisbury screen can be improved. Theoretically the bandwidth of Jaumann absorber may be three times that of a single Salisbury screen [4]. Figure 8 shows the reflected power versus frequency for absorbers with numerous resistive sheets. It is evident that theoretically the frequency bandwidth is increased with the increase in the number of layers. For this illustration, the spacing between sheets is at 7.5 mm (a quarter wavelength at 10 GHz) and a quadratic resistance taper is used. Note that the four-sheet structure has about four times the fractional bandwidth of a single layer [1]. In Table 1 the relationship between the number of sheets, fractional bandwidth and total thickness is listed.

Bandwidth of Jaumann Absorbers		
Number of sheets	Fractional Bandwidth	Total Thickness (cm)
1	0.27	0.75
2	0.55	1.50
3	0.95	2.25
4	1.16	3.00

Table 1. The number of sheets versus fractional bandwidth (From [1]).

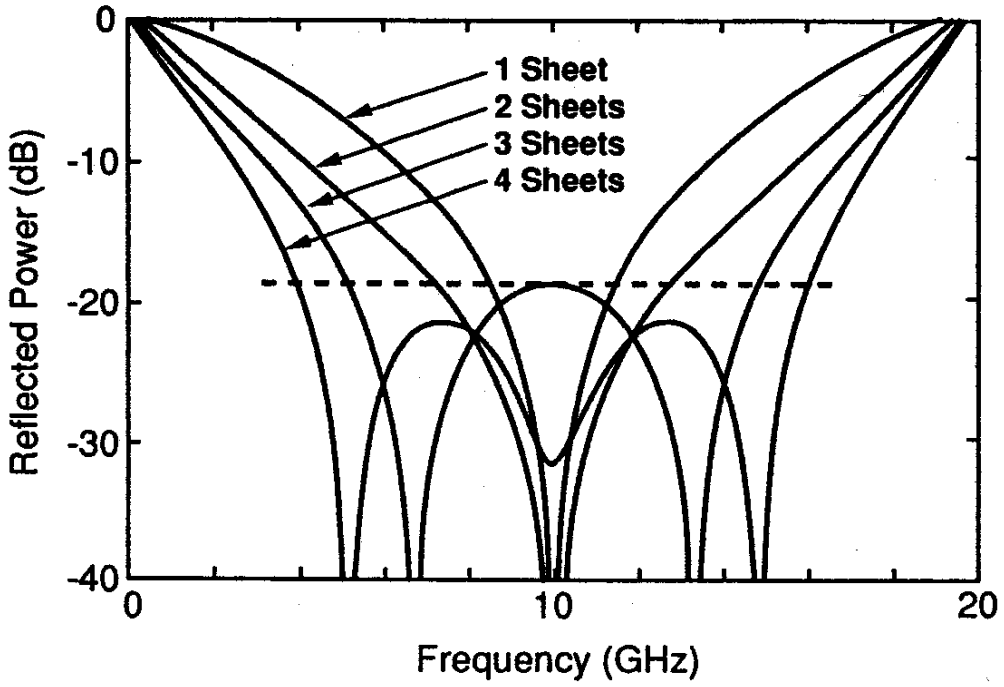

Figure 8. The predicted performance of Jaumann multilayer absorbers (From [1]).

The graded dielectric absorbers are constructed of discrete layers with properties changing from layer to layer. A technique for reducing the reflection from the front face of a flat absorber is to produce a material whose intrinsic impedance is very close to unity by employing conductivity gradient up to certain degree. Two common examples are the hair-type and the carbon-loaded low density foam absorbers [1].

Since the structural property and RCSR performance of the hair-type absorbers are poor compared to pyramidal absorbers and graded dielectrics, hair-type absorbers are not widely used.

Carbon-loaded foam using geometric transition from a free space into a lossy media is another type of graded absorber. The transition to the lossy medium establishes a dielectric gradient and the reflections are reduced. This type of absorber is usually in the form of pyramids or wedges of rubber or plastic foam which is loaded with an electrically lossy materials such as carbon. In Figure 8 a sketch of such absorber is shown. Geometric absorbers are generally not used in target RCSR applications because of the large volume they occupy.

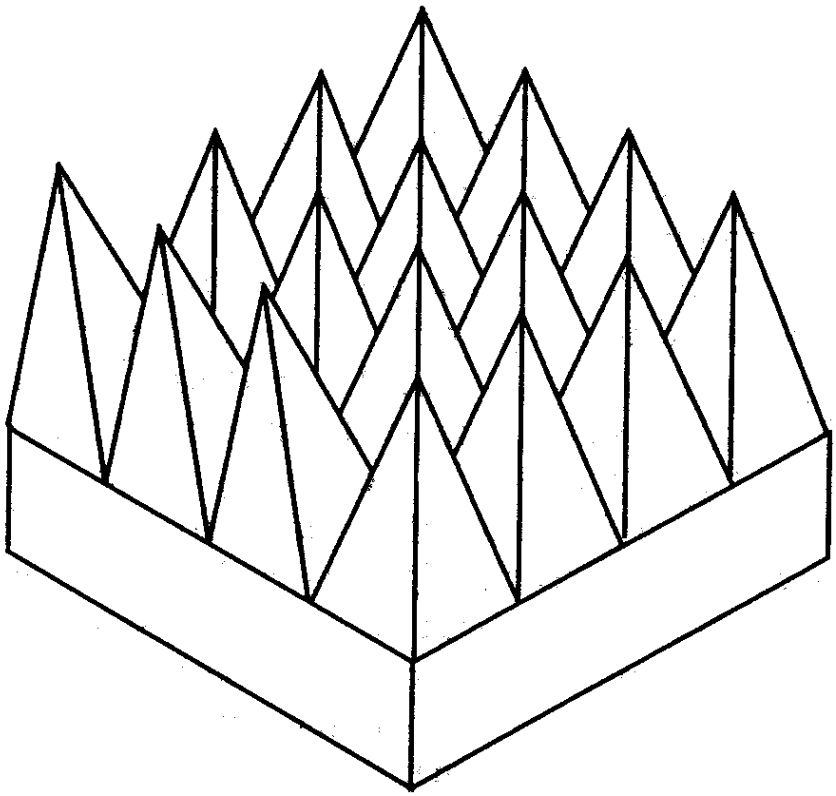

Figure 9. Geometric transition absorber (From [1]).

E. MAGNETIC RAM

Magnetic RAM, such as ferrite slabs, have distinct advantages over dielectric absorbers, since magnetic RAM only requires one-tenth of the thickness of the dielectric absorber to achieve the same RCS reduction. Magnetic materials have relative permeabilites different than that of free space. To this point, the RCSR approaches have employed a complex relative permittivity with a non-magnetic material ($\mu_r = 1 + j0$). Clearly the intrinsic impedance of such a material is $377/\varepsilon_r$ and the index of refraction is $\sqrt{\varepsilon_r}$. Having the relative permeability other than one, enables further modification of intrinsic impedance and index of refraction, and consequently the resulting absorption performance gets better.

The magnetic materials that are available for use in RAM generally have relative permittivities higher than their relative permeabilities. Therefore, practically speaking,

pure magnetic (non dielectric) materials with $\varepsilon_r = 1 + j0$, do not exist [1]. Research in materials science has lead to artificial materials constructed of dielectric and magnetic components that have a wide range of ε_r and μ_r. In most applications, iron and components of iron are most preferred. The two most common materials employed in RAM are carbonyl iron and ferrites suspended in a dielectric.

The main difference between magnetic and electric material is the thickness required for the first resonance. Magnetic RAM, despite of the fact that it is heavy, can operate at low frequencies with reasonable thickness. The thickness required for a magnetic RAM to obtain low-frequency coverage down to 100 MHz, is much less than one tenth that of a dielectric absorber.

In reference [6] it is shown that for a Dallenbach layer, the lowest possible reflection (Γ_0) is related to the widest operating band ($\Delta\lambda$) by

$$\frac{\Delta\lambda}{\lambda_0} = \frac{2\Gamma_0}{\left(\pi d / \lambda_0\right)\left|\varepsilon_r - \mu_r\right|} \tag{3.17}$$

where λ_0 is the center frequency. The bandwidth for a thin layer $(t \ll \lambda_0)$ becomes

$$\Delta\lambda \approx \frac{32}{\pi}\Gamma_0 \,\mathrm{Re}\{\mu_r\} t. \tag{3.18}$$

This illustrates the necessity for a high permeability layer if it is to be thin and $\Delta\lambda$ large.

The loss increases at low frequencies with the increasing μ_r. On the other hand, the relative dielectric constant changes linearly with the frequency increase (Figure 10). As the frequency increases the magnetic properties do not affect the loss, however the electric properties start to contribute to loss.

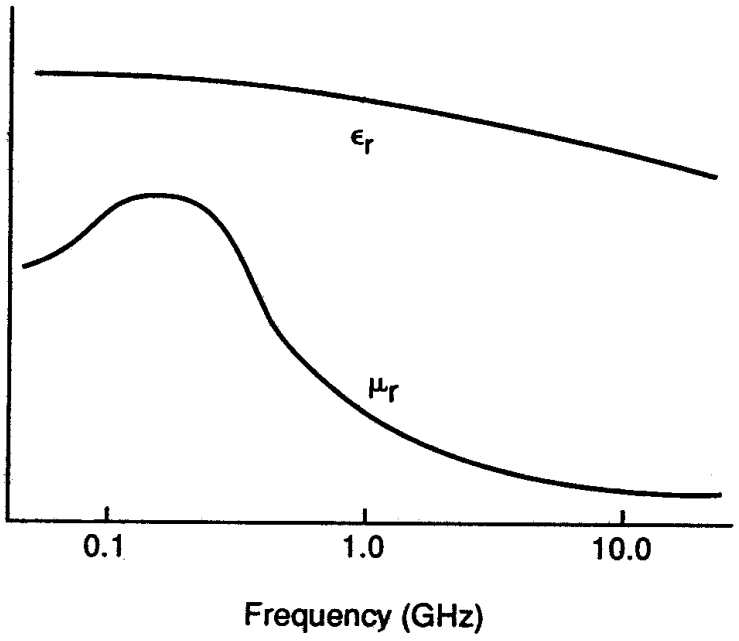

Figure 10. Schematic illustration of the frequency behavior of ferrites. (From [1])

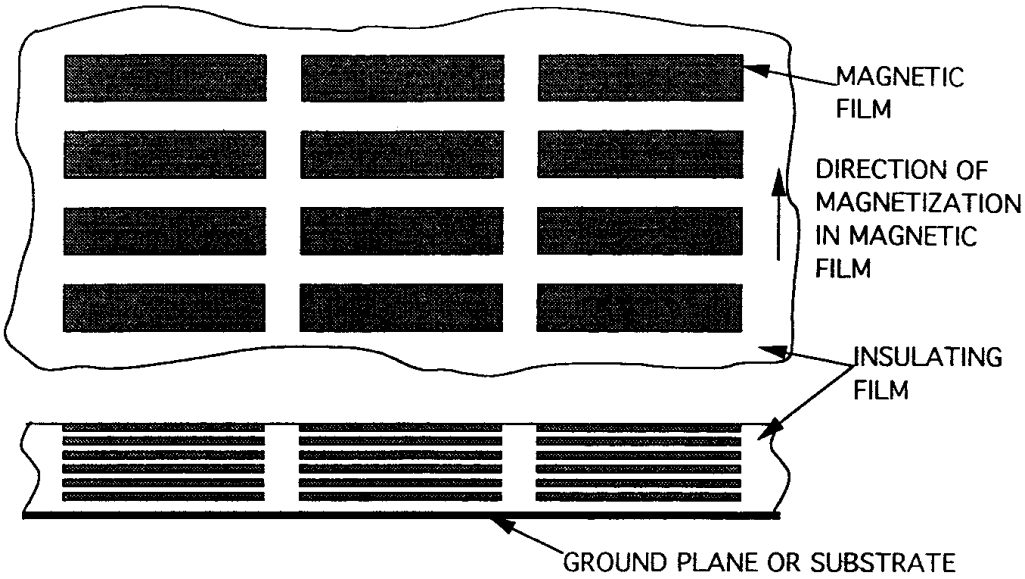

Figure 11. Thin-film magnetodielectric as used in circuit applications (From [1])

The suspended particle approach to constructing magnetic material can be applied on a macroscopic scale. The magnetic losses can be manipulated by arranging layers of thin magnetic films in dielectric, as shown in Figure 11. These are referred to as thin-film

magnetodielectrics (TFM). The thin films increase the surface area exposed to the wave and circumvent the skin depth limitations encountered with a conducting magnetic material [2].

F. MATCHED SURFACE RAM

The discussions in Section D show that choosing the appropriate dielectric and magnetic properties of a material will produce zero specular reflection. Two different concepts have been introduced in specular reflection reduction applications: (1) matched characteristic impedance, and (2) matched wave impedance.

The goal is to find a material whose impedance in combination with backing material is equal to the intrinsic impedance of the free space. In other words, the relative dielectric constant of the material and the relative magnetic permeability of the material is equal to each other at every point. Musal and Smith [7] refer to concept as the "matched-characteristic impedance" approach in which there is no front-surface reflection for normal incidence from the material layer. Making the layer thick enough so that internal attenuation along the round-trip path through the material reduces the emerging wave to an acceptably low amplitude eliminates any reflection from the backing material.

The second approach in specular reflection reduction is the "matched wave impedance" approach [7]. The idea is that the wave impedance at the front surface of the reflector-backed material layer is made equal to the intrinsic impedance of the free space, thus producing no reflection at all. In this study, following chapters are dedicated to the concept of matched wave impedance approach for theoretical analysis and applications in various materials.

G. OTHER RADAR ABSORBING STRUCTURES

Traditional studies of RAM have always considered absorber as an "add on" material with its own specifications and properties, which cause additional weight and extra design considerations. However, communities like aviation persistently aim to cut

down on weight, and have started designing RAM as an integral composite part of the object. This approach may involve combining several absorber designs, and therefore are called hybrid RAMs.

An example of a hybrid RAM for broadband operations that includes low-frequency applications, which has a front layer of Jaumann absorbers or graded dielectric and back layer material of magnetic material. At low frequencies the magnetic material is clearly superior (Figure 10) and at microwave frequencies the front layers of dielectric RAM would provide the attenuation. Figure 12 provides predicted data for a three-layer Jaumann absorber, a four-layer graded dielectric absorber (dipped core honeycomb, for example), and a hybrid formed by combining a Jaumann with a graded dielectric. Each layer is 7.55mm. thick, so the total RAM thickness is 3 cm. Note that the use of the combined techniques provides both improved low-frequency performance and good performance through K_u band [1].

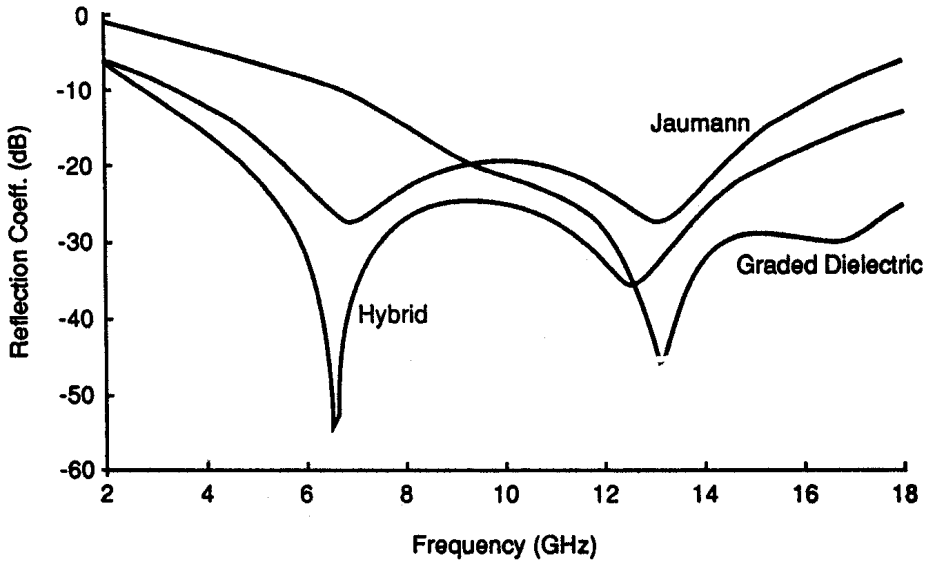

Figure 12. Reflection coefficient as a function of frequency (From[1])

The circuit analog technique introduces the idea of representing the geometrical patterns in terms of effective resistance, capacitance, and inductance, and then equivalent circuit techniques are used in the design of the resulting absorber.

Salisbury screens and Jaumann absorbers employ resistive sheets that only have real part of the admittance. Clearly, flexibility can be obtained if the sheets have susceptance as well as conductance. Figure 13 shows circuit analog geometries like dipoles, crosses or triangles. In any event, the reason for employing circuit analog sheets rather than simple resistive sheets in an absorber is to provide increased bandwidth through increased control of the impedance properties of the lossy material.

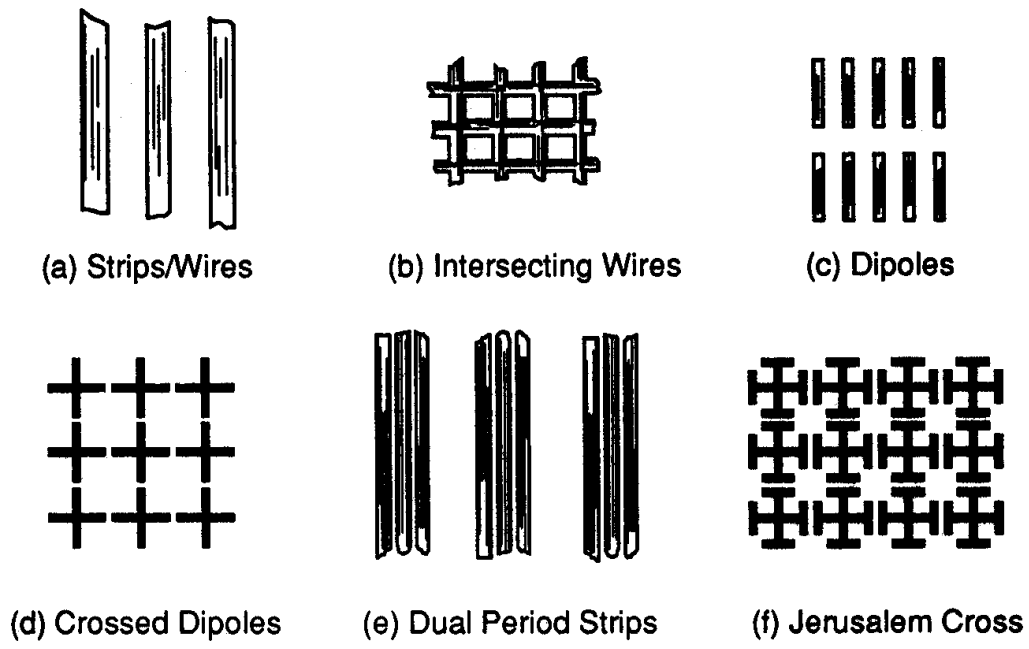

Figure 13. Typical circuit analog element geometries (From [1])

H. NONSPECULAR RAM

The nonspecular returns are from surface traveling waves, edge waves, creeping waves, the gaps, cracks and edge diffractions. In order to deal with the surface wave and traveling waves returns two different approaches have been employed: (1) magnetic and dielectric surface coatings and (2) tapered resistive sheets.

Magnetic RAM is employed most effectively in close contact with a perfectly conducting surface where the magnetic field has its highest value. It has been known that

a thin coating of magnetic RAM could effectively reduce traveling and creeping wave returns [1]. The approach to the calculating of the effects of a surface coating on traveling wave amplitude follows the analysis of lossy surface wave transmission line.

The incident wave has an electric field in the $x-z$ plane, and the associated magnetic field in free space is given by

$$H_{yo} = H \exp[j(\beta_o z - h_o x)] \tag{3.18}$$

with the propagation constants β_0 and h_o such that

$$\beta_o^2 + h_o^2 = k_o^2 = (2\pi / \lambda_o)^2 \tag{3.19}$$

where λ_0 is the free space wavelength. A similar set of equations holds for the magnetic field inside the layer, with the values of β, h and λ depending on the thickness of the layer and the properties of the coating (i.e., $k_1 = k_0\sqrt{\mu_1\varepsilon_1}$). For the guided wave case, the impedance at the boundary must match for the two waves (the free-space wave and the one in the coating layer) [1]. A matched condition occurs with $Z_{0x} = Z_{1x} = Z_s$, where Z_{ox} is 377Ω, and Z_s is the surface (or input) impedance of the coating. Matching impedances and solving for the equivalent of Equation (3.18) in the material gives

$$h = k_0 Z_s / 377. \tag{3.20}$$

The value of *h* can then be substituted into Equation (3.19) to find β.

The parameter of interest is the attenuation of the z-traveling wave provided by the coating, and that is given by the imaginary part of the β, where

$$\beta = (2\pi / \lambda_0)(1 - Z_s^2 / 377^2)^{1/2}. \tag{3.21}$$

The surface impedance of the layer will depend on the angle of the incidence of the incoming wave. However, for large ε and μ values, the direction of the refracted ray in the material layer will be very close to the normal, regardless of the incidence angle. The attenuation per wavelength of travel in the z-direction in the layer is then given by

$$L = 8.69 \,\mathrm{Im}\{\beta\} \text{ dB}/\lambda_0 \tag{3.22}$$

In Figure 14, the surface wave attenuation per wavelength of propagation as a function of layer thickness for a thin magnetic RAM coating is shown. The attenuation rises rapidly with increasing thickness, but peaks and then begins rapidly decreasing. The decrease occurs as the surface impedance begins to go from inductive to capacitive, and layer begins to shed, rather than trap, a surface wave. The peak loss for the material shown is about 28 dB/λ_0 and occurs for a layer thickness of about $0.037\,\mathrm{dB}/\lambda_0$, or 1 cm at 1 GHz [1].

Scattering also arises from the impedance discontinuities on a body. Those discontinuities can be due to changes in materials (e.g., transition from a metal fuselage to a nonconducting canopy), or they can be geometric (a discontinuity in any derivative of the surface contour provides a theoretical opportunity for backscatter, although discontinuities with radii of curvature greater than a wavelength can generally be ignored). Clearly, two of the most severe discontinuities possible are sharp edges and corners, but they are also structures that often appear on vehicles designed for low RCS because of their natural occurrence in application of the shaping rules [1].

Edges and corners are important constituents in three different types of scattering. First, perpendicular to a leading edge for parallel polarization or a trailing edge for perpendicular polarization, there is an edge diffraction return given as $\sigma \approx L^2/\pi\ \mathrm{m}^2$. Corners provide a lower level, but relatively isotropic, diffraction return. Also, edges and corners provide the area from which physical optics end-region returns rise. Finally, edges and corners provide discontinuities that reflect surface traveling waves and edge waves, giving the opportunity for return in the backscatter direction [1].

Therefore, the treatment of edges can potentially reduce threat sector RCS levels for all three of the major scattering mechanisms expected in a vehicle shaped for low RCS. As in the design of specular RAM, wideband edge treatments must provide slowly varying impedance to taper the transition between free space and the body being treated.

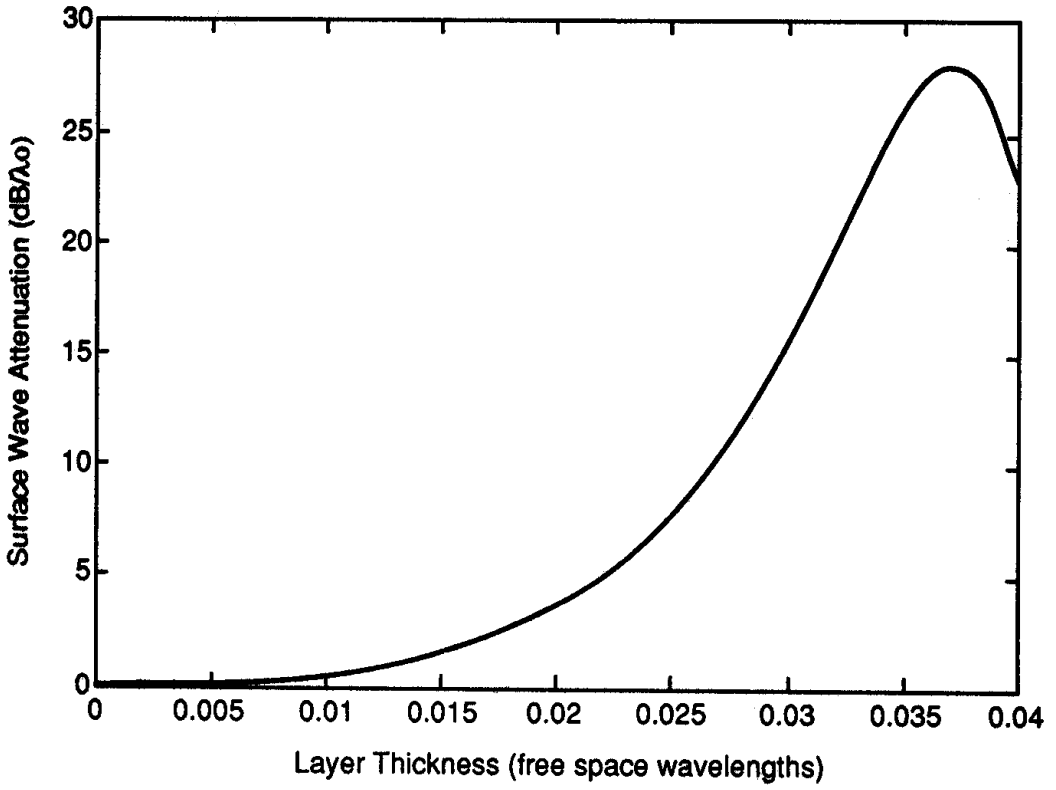

Figure 14. Surface wave attenuation as a function of layer thickness (From [1])

I. SUMMARY

The main objective in radar absorbing material design is to set the RAM parameters in order to allow the wave to enter the layer and then provide sufficient loss to absorb the energy within RAM thickness. The two requirements generally conflict, since high-loss materials often have intrinsic impedances different that of free-space and thus suffer high front-face reflections.

Two basic solutions are applied to address the problem. Tapering the loss from the front to the back of the absorber with Jaumann, graded electric and geometric transition absorbers is one of the solutions. The major disadvantage of these methods is the increased thickness for low frequencies. The other solution is the employment of tuned but high loss materials. The purpose is to establish a matched transmission line

between free space and the material in order to cancel out the reflections. Magnetic materials are best for this condition but in practice the frequency bandwidth is quite limited. In order to increase the bandwidth, the hybrid materials can be used. In spite of the fact that the hybrid materials can provide significant performance in a reasonable thickness, problems in production and maintenance and high cost are the disadvantages.

This chapter is dedicated to describing various types of RAM and discussions of their performance characteristics. The crucial issue in RAM employment is the trade-off study between cost, maintenance, performance, and ease of manufacturing. A systems engineering study will dictate the most reasonable solution for a particular target and its intended mission.

THIS PAGE INTENTIONALLY LEFT BLANK

IV. UNIVERSAL DESIGN CHART FOR SPECULAR ABSORBERS

A. INTRODUCTION

Theoretical analysis in Chapter III clearly shows that the material configuration and electromagnetic parameter values of a single homogeneous layer of dielectric/magnetic material can produce zero specular reflection.

In this chapter the analysis of zero specular reflection absorbers is discussed. The equations related to the specular absorbers are analyzed based on the transmission line approach. Then, numerical solutions of the equations are used to generate universal design charts for zero specular reflection layers.

B. EQUATIONS FOR ZERO SPECULAR REFLECTION

Two different conceptual approaches have been applied in the specular reflection reduction application due to [7]. The first is the *matched-characteristic impedance* concept, in which the intrinsic impedance of the material is made equal to the intrinsic impedance of free space. Consider a layer of such medium placed in front of a conducting plate, the other side of the layer forming a plane interface with free space and illuminated by normally incident plane wave as in Figure 15. If the layer medium is matched to free space, in other words, if the relative dielectric constant and relative magnetic permeability of the material are equal to each other, then there is no front surface reflection from the material. The incident wave is attenuated to a very low amplitude by the round-trip path in an absorption layer that is thick.

The second concept is *matched wave impedance,* in which the wave impedance at the front surface of the reflector backed material layer is made equal to the intrinsic impedance of free space, thus producing no reflection at all. This approach forms basis to the studies in this thesis. It is theoretically possible to design a combination dielectric/magnetic absorber layer that will results in zero reflection at a specific wavelength. Referring to Figure 15, the six design parameters are wavelength (λ), layer thickness (t), the real part of dielectric constant (ε'), the imaginary part of dielectric

constant (ε''), the real part of permeability (μ'), and the imaginary part of permeability (μ'').

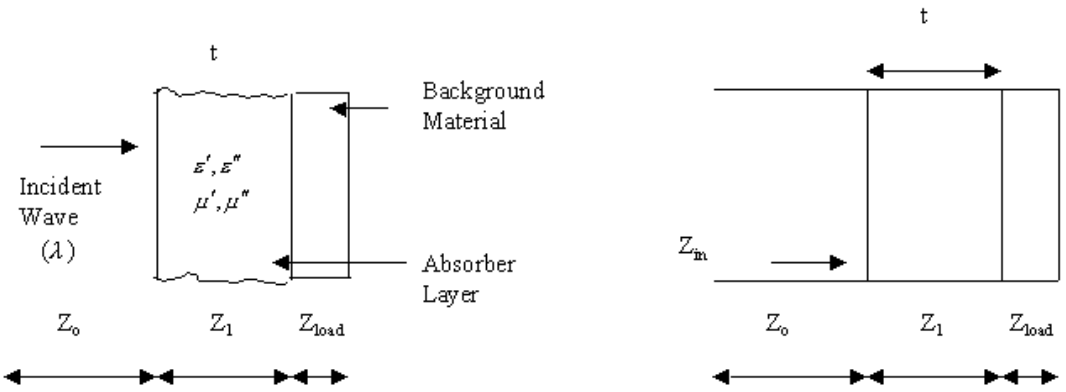

Figure 15. Specular Reflection

An incident plane wave, having electric field $\overrightarrow{E_i}$ and magnetic field $\overrightarrow{H_i}$, illuminates the platform. The reflected wave having electric field $\overrightarrow{E_r}$ and magnetic field $\overrightarrow{H_r}$ results. The wave impedance at any plane parallel to the material is defined by

$$Z = \frac{\left|\vec{E}_{\tan}\right|}{\left|\vec{H}_{\tan}\right|} \tag{4.1}$$

where $\vec{E}_{\tan}$ is the tangential electric field component and $\vec{H}_{\tan}$ is the tangential magnetic field component. The ratio of the reflected wave amplitude to the incident wave amplitude is reflection coefficient (Γ) defined by

$$\Gamma = \frac{Z_{in} - Z_o}{Z_{in} + Z_o} \tag{4.2}$$

$$\Gamma = \frac{Z_{in}/Z_o - 1}{Z_{in}/Z_o + 1} \tag{4.3}$$

It can be seen from Equation (4.3) that if Z_{in}/Z_0 equals to 1 then the reflection coefficient on the surface will be zero. The impedance at the front surface of the reflector backed material layer is made equal to the intrinsic impedance of free space, thus producing no reflection.

In our case, based on Figure 15, the transmission line equation can be applied for a normally incident wave so Z_{in} can be defined as

$$Z_{in} = Z_1 \frac{Z_{load} + jZ_1 \tan(\beta t)}{Z_1 + jZ_{load} \tan(\beta t)} \tag{4.4}$$

where Z_{load} represents the background object (the platform material) and Z_1 represents the layer (absorbing material), where

$$\begin{aligned} Z_{load} &= \sqrt{\frac{\mu_o(\mu_r' - j\mu_r'')}{\varepsilon_o(\varepsilon_r' - j\varepsilon_r'')}} \\ Z_1 &= \sqrt{\frac{\mu}{\varepsilon}}. \end{aligned} \tag{4.5}$$

Note that the propagation constant is complex in this representation

$$\beta = \omega\sqrt{(\varepsilon_r' - j\varepsilon_r'')(\mu_r' - j\mu_r'')} \tag{4.6}$$

If we normalize each term of Equation (4.4) by Z_0 and then Z_{in}/Z_o equal to 1 is the condition for no reflection for a given Z_{load}. The resulting equation turns out to be a transcendental equation description of the required relationship between the six system parameters, which can be evaluated numerically. The normalized Z_{load} and Z_1 are

$$\begin{aligned} Z_{load}/Z_0 &= \sqrt{\frac{1}{\varepsilon_r' - j\varepsilon_r''}} \\ Z_1/Z_0 &= \sqrt{\frac{\mu_r' - j\mu_r''}{\varepsilon_r' - j\varepsilon_r''}}. \end{aligned} \tag{4.7}$$

Since the real and imaginary parts of Z_{load} are known, the equation can be evaluated by using a computer-implemented complex root finder algorithm to find numerical values of Z_1 and therefore the dielectric constant and permeability.

Solutions to this equation can be found using Mathematical software packages like Mathcad and Matlab. Mathcad's "*find*" function solves for N nonlinear equations in N unknowns. When the *"find"* function is used, Mathcad's Autoselect feature automatically determines the type of equation and then tries appropriate algorithms to find a valid solution. For nonlinear equations, the autoselect uses the Conjugate Gradient Solve. If that fails to converge, the Levanberg-Marquart Solver is used. If that fails too, the Quasi-Newton Solver is used. To determine whether a solution is valid, the solvers use the built-in variable values of Convergence Tolerance (TOL) and Constraint Tolerance (CTOL). CTOL specifies how closely constraints must be met for a solution to be considered valid. The smaller the CTOL is, the more precise the solution may be. TOL specifies how accurate the solution must be. The default values of built-in functions are 0.001, however most the current problem the values are set to 10^{-8} in order to be more precise.

C. MATCHING LAYER FOR $Z_{load} = 0$

The first implementation of the Equation (4.4) was to find lossy dielectric magnetic layers that produce zero specular reflection. The background material is set to be a perfect conducting material ($Z_{load} = 0$). Equation (4.4) is simplified to

$$Z_{in} = jZ_1 \tan(\beta t). \tag{4.8}$$

If we normalize Equation (4.5) by Z_0 to get Z_s

$$\begin{aligned} Z_{in}/Z_o &= j\frac{Z_1}{Z_0}\tan(\beta t) \\ Z_s &= j\sqrt{\frac{\mu_r' - j\mu_r''}{\varepsilon_r' - j\varepsilon_r''}}\tan(\omega\sqrt{\mu_o\varepsilon_o}\sqrt{\mu_r\varepsilon_r}) \end{aligned} \tag{4.9}$$

then Equation (4.7) can be written as

$$Z_s = j\sqrt{\frac{\mu_r' - j\mu_r''}{\varepsilon_r' - j\varepsilon_r''}}\tan[2\pi(t/\lambda)\sqrt{(\mu_r' - j\mu_r'')(\varepsilon_r' - j\varepsilon_r'')}]. \quad (4.10)$$

In order to simplify the equation, the numerator and denominator of the first part of the equation are multiplied by t/λ and the equation is rewritten as

$$Z_s = j\sqrt{\frac{(\mu_r' - j\mu_r'')(t/\lambda)}{(\varepsilon_r' - j\varepsilon_r'')(t/\lambda)}}\tan\left[2\pi(t/\lambda)\sqrt{(\mu_r' - j\mu_r'')(\varepsilon_r' - j\varepsilon_r'')}\right]. \quad (4.11)$$

For convenience a new set of variables can be defined:

$$\begin{aligned} x &= (t/\lambda)\,\mathrm{Re}[\mu] = (t/\lambda)\mu_r' \\ y &= (t/\lambda)\,\mathrm{Im}[\mu] = (t/\lambda)\mu_r'' \\ a &= (t/\lambda)\,\mathrm{Re}[\varepsilon] = (t/\lambda)\varepsilon_r' \\ b &= (t/\lambda)\,\mathrm{Im}[\varepsilon] = (t/\lambda)\varepsilon_r''. \end{aligned} \quad (4.12)$$

Equation (4.11) is redefined as

$$Z_s = j\sqrt{\frac{(x - jy)}{(a - jb)}}\tan\left[2\pi\sqrt{(x - jy)(a - jb)}\right]. \quad (4.13)$$

Figure 16 shows the universal design chart that depends on six independent parameters which are combined into the four parameter groups in Equation (4.12). The last parameter is the dielectric loss tangent $\tan\delta_\varepsilon$. The entire chart represents combinations of the four parameter groups that constitute a zero-reflection absorber with the exception of the $\tan\delta_\varepsilon = 0$ contour. The values of $(t/\lambda)\,\mathrm{Re}[\mu]$ and $(t/\lambda)\,\mathrm{Im}[\mu]$ are read from the abscissa and ordinate scales, respectively. The values of $(t/\lambda)\,\mathrm{Re}[\varepsilon]$ are read by interpolation between bounding contours of constant values of $(t/\lambda)\,\mathrm{Im}[\varepsilon]$ (red lines). The values of $\tan\delta_\varepsilon$ are read by interpolation between bounding contours of constant values of $\tan\delta_\varepsilon$ (blue lines).

There are three distinctly different parameter regimes depicted on the chart. The single coalesced curve at the left side represents thin (less than "quarter-electrical-wavelength" thick) absorbers (magnetic Salisbury screens). Going to the extreme left on this curve requires values of dielectric constant that are less than unity, which is not

physically realistic. The region across the top of the chart above the coalesced curve represents the matched characteristic-impedance absorbers. Although the chart displays $\tan\delta_\varepsilon$ contours only for values up to 10, in fact, the entire region progressing from right to left could be filled with a sequence of similar curves of progressively higher $\tan\delta_\varepsilon$ values. The lower right region of the chart represents, in a generalized sense, resonant quarter-electrical-wavelength-thick absorbers [7].

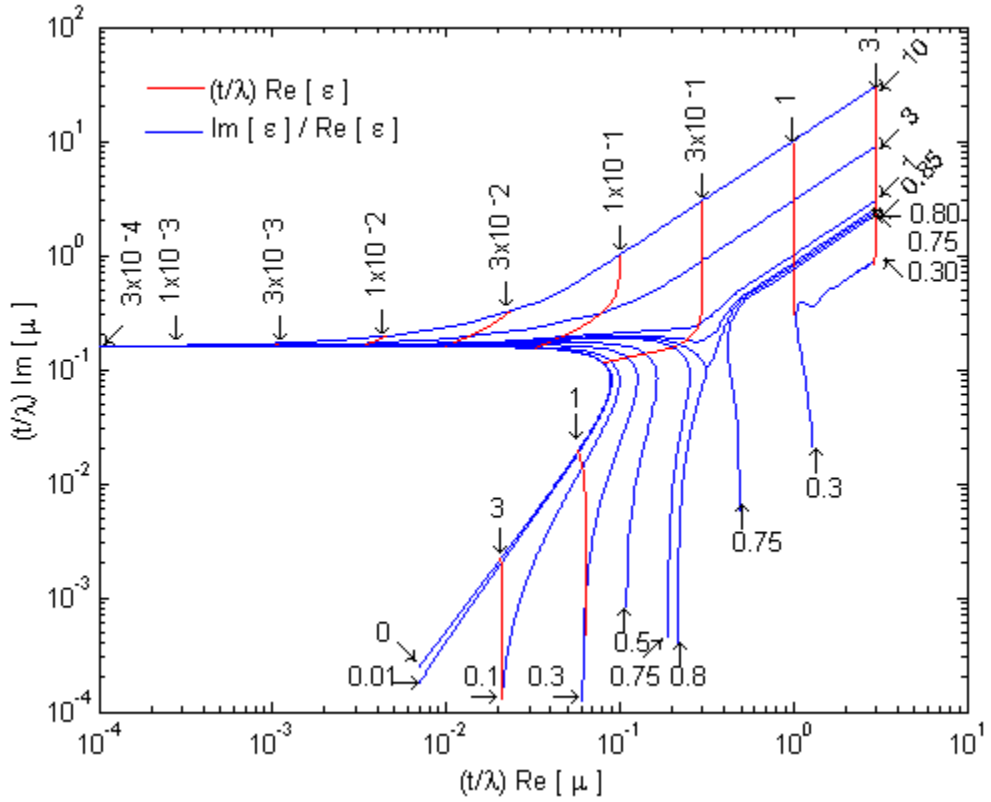

Figure 16. Universal Design Chart for Zero Specular Reflection Absorber Layer ($Z_{load} = 0$)

The region where the dielectric loss tangent is less than 0.3 and $\mathrm{Im}[\mu] \geq 3\,\mathrm{Re}[\mu]$, the parameters are approximated by

$$(2\pi t/\lambda)\,\mathrm{Im}[\mu] = 1 \tag{4.14}$$

$$\mathrm{Re}[\varepsilon] = 3\,\mathrm{Re}[\mu] \tag{4.15}$$

Equation (4.14) determines the required layer thickness in terms of the radiation wavelength and only the imaginary part of the magnetic permeability at that wavelength. Equation (4.15) shows the relationship between real parts of magnetic permeability and dielectric constant. In order to have the reflection close to zero this equation must be satisfied. The required thickness is also dependent on this equation.

In the upper part of the chart, where $(t/\lambda)\,\mathrm{Im}[\mu] \geq 1$, the relationship can be defined as

$$\mathrm{Re}[\varepsilon] = \mathrm{Re}[\mu] \tag{4.16}$$

$$\tan\delta_{\varepsilon} = \tan\delta_{\mu} \tag{4.17}$$

where magnetic loss tangent equals to

$$\tan\delta_{\mu} = \frac{\mathrm{Im}[\mu]}{\mathrm{Re}[\mu]}. \tag{4.18}$$

Equations (4.16) and (4.17) are equivalent to the statement (complex) that $\varepsilon = \mu$, which is the definition of a matched-characteristic impedance absorber, in which the intrinsic impedance of the material is made equal to the intrinsic impedance of free space. Thus, for all practical purposes, a matched-characteristic impedance absorber is equivalent to a zero reflection absorber when $(t/\lambda)\,\mathrm{Im}[\mu] \geq 1$.

The lower right region of the chart exhibits a complicated relationship between the parameter groups that constitute a zero-reflection absorber. This region includes the quarter electrical wavelength thick absorber. The lower part of the chart consists of two subregions. In the left subregion, between $\tan\delta_{\varepsilon} = 0$ and $\tan\delta_{\varepsilon} = 0.8$ contours, the thickness of the layer is approximately one-quarter electrical wavelength [7]. It can be expressed as

$$(4t/\lambda)\,\mathrm{Re}[(\mu\varepsilon)^{1/2}] \cong 1. \tag{4.19}$$

Equation (4.19) is most accurate near the $\tan\delta_{\varepsilon} = 0$ contour. Near the bottom of the chart, where dielectric loss dominates, the relationship is

$$(\pi t/\lambda)\,\mathrm{Im}(\varepsilon) \cong 1. \tag{4.20}$$

D. MATCHING LAYER FOR $Z_{load} = 120\pi$

The agreement of the computed plot with the published data for the PEC backing material serves as a validation of the numerical solution. Next, the background material is made equal to the impedance of air, which is 377 or 120π ohms. In this special case

$$Z_{load} = Z_o. \tag{4.21}$$

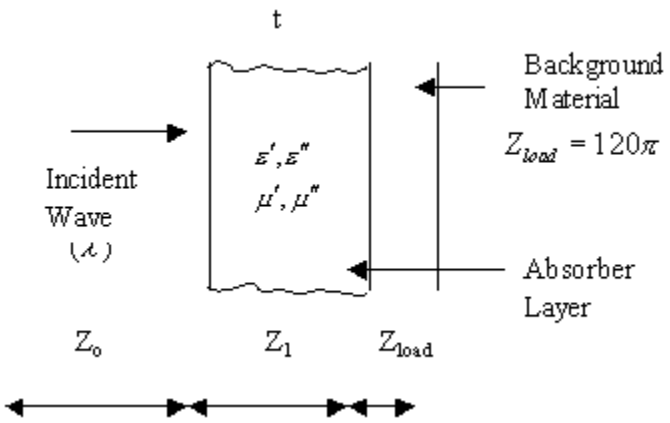

Figure 17. Matched Load Layer

If Equation (4.4) is recalled

$$Z_{in} = Z_1 \frac{Z_{load} + jZ_1 \tan(\beta t)}{Z_1 + jZ_{load} \tan(\beta t)}$$

then, the equation can be rewritten as

$$Z_{in} = Z_1 \frac{120\pi + jZ_1 \tan(\beta t)}{Z_1 + j120\pi \tan(\beta t)} \tag{4.22}$$

where

$$Z_{load} = 120\pi \cong 377. \tag{4.23}$$

In Figure 18, the universal design chart is shown where the background material, Z_{load} is equal to Z_0. As shown in Figure 16, the results depend on six independent parameters, which are combined into the four parameter groups shown in Equation

(4.12). The entire chart represents combinations of the four parameter groups that constitute a zero-reflection absorber with the exception of the $\tan\delta_\varepsilon = 0$ contour.

The chart has two regions, in the upper part of the chart, where $(t/\lambda)\,\mathrm{Im}[\mu] \geq 1$, the relationship can be defined as,

$$\mathrm{Re}[\varepsilon] = \mathrm{Re}[\mu] \tag{4.24}$$

$$\tan\delta_\varepsilon = \tan\delta_\mu \tag{4.25}$$

In the lower left region where $(t/\lambda)\,\mathrm{Re}[\varepsilon] \leq 0.75$, the curves are all meet at the point where $(t/\lambda)\,\mathrm{Re}[\mu] = (t/\lambda)\,\mathrm{Re}[\varepsilon] = 0.2$ and the $\tan\delta_\varepsilon = 0.3$ cuts through all the lines in this region. Note that the upper right region is essentially unchanged from Figure 16. That is because the layer is highly lossy in this region, so the waves never reach the backing material, and therefore its composition is irrelevant.

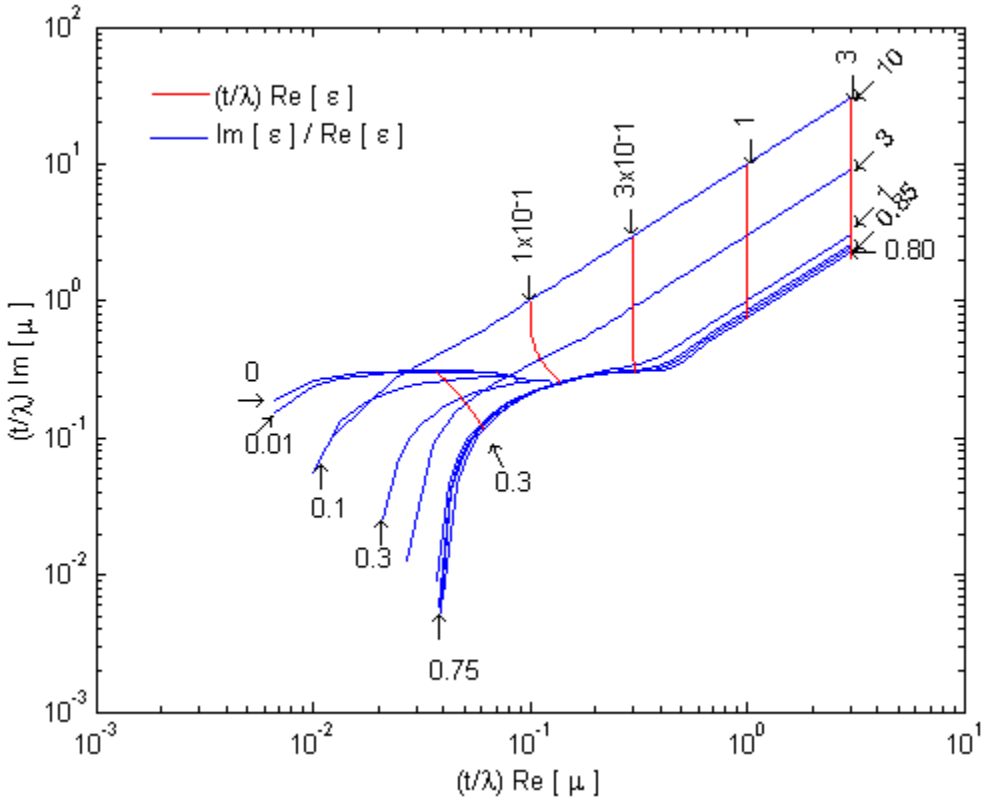

Figure 18. Universal Design Chart for Zero Specular Reflection Absorber Layer ($Z_{load} = 120\pi$)

E. GRAPHITE BACKING MATERIAL

Graphite has become a popular material in aircraft construction. Therefore it is desirable to investigate the types of coatings that could be used to reduce the reflection from the graphite. First, however the characteristics of graphite are discussed.

1. Definition

Graphite fibers are group of fibrous materials comprising essentially elemental carbon. The graphite fibers themselves are composites in that only part of the carbon present has been converted to graphite in tiny crystalline platelets specially oriented with respect to the fiber axis. The higher the graphite content, the stiffer the fiber, but lower the strength. The most significant properties are: light-weight, high-strength, and high-stiffness [9].

2. Applications

Composite materials, especially graphite/epoxy are being used to a significant extent in present-day aircraft structures. The most common applications of graphite in aircraft structures are for the skin of wings, tails, and control surfaces. Generally, such skins are made in the form of monolithic laminates, i.e., without discrete stiffeners such as stringers on their inner surfaces [8].

In Table 2, the aircraft applications of graphite are listed.

Aircraft	Application
F-14	Boron/epoxy horizontal tail skins
F-15	Boron/epoxy horizontal and vertical tail skins
F-16	Graphite/epoxy horizontal and vertical tails skins and control surfaces
F/A-18	Graphite/epoxy horizontal and vertical tails skins and control surfaces
AV-8B	Graphite/epoxy wing, forward fuselage and control surfaces
Boeing 757	Graphite/epoxy control surfaces
X-29	Graphite/epoxy wing skins

Table 2. Aircraft Applications of Composite Materials (From[8]).

3. Matching Layer for Graphite

In this application, the background material impedance, Z_{load}, is for graphite and Equation (4.4) is redefined based on graphite's dielectric and magnetic properties in order to solve the equation from a zero reflection absorber layer. Graphite properties are shown in Figure 19.

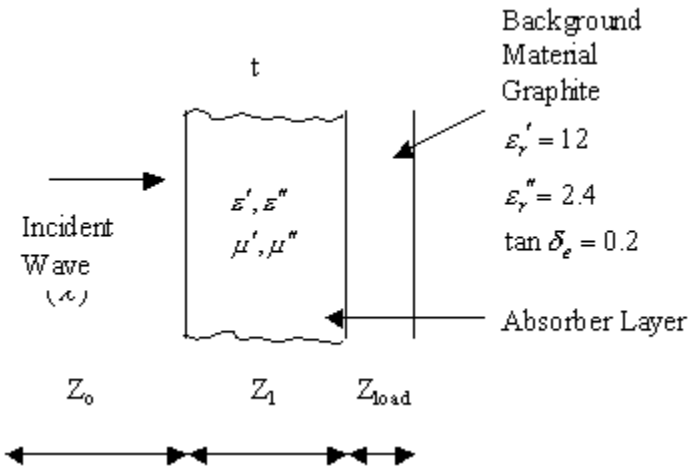

Figure 19. Specular Reflection for Graphite

The Z_{load} normalized by Z_o can be expressed in terms of graphite's dielectric and magnetic properties as

$$Z_{load-graphite} = \sqrt{\frac{1}{(\varepsilon_r' - j\varepsilon_r'')}} = \sqrt{\frac{1}{(12 - j2.4)}} \tag{4.26}$$

Equation (4.4) is applied to this case giving

$$Z_{in} = Z_1 \frac{\sqrt{1/(12 - j2.4)} + jZ_1 \tan(\beta t)}{Z_1 + j\sqrt{1/(12 - j2.4)} \tan(\beta t)} \tag{4.27}$$

Figure 20 shows the universal design chart for graphite, obtained by solving this equation numerically.

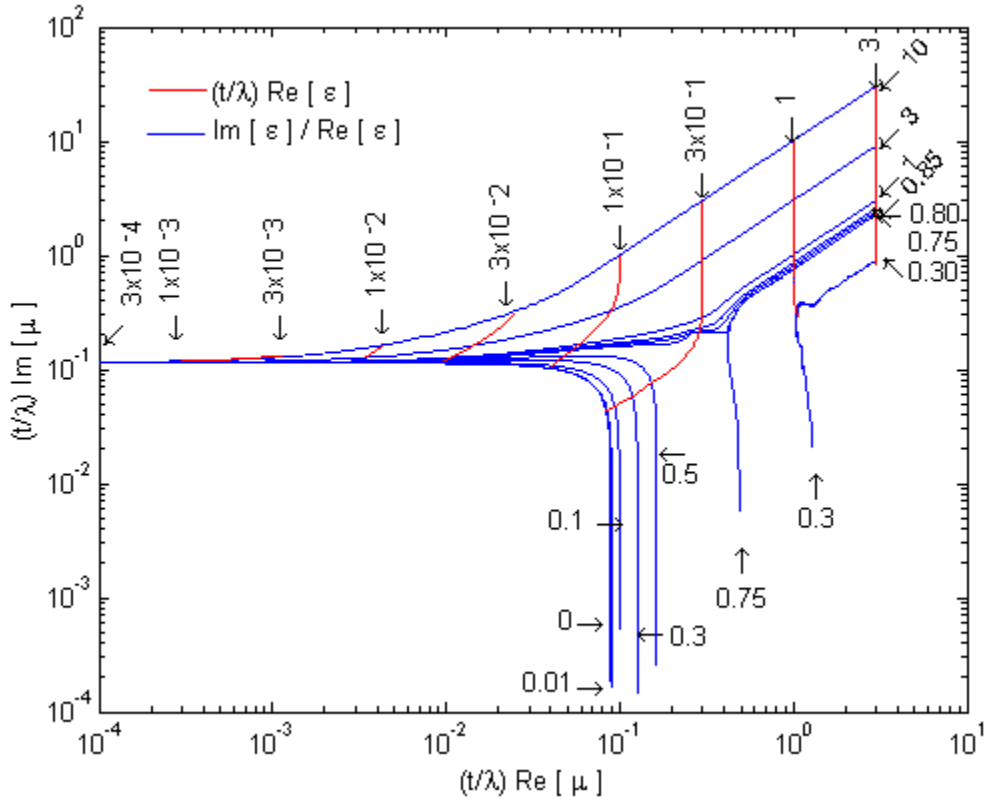

Figure 20. Universal Design Chart for to Graphite

The chart has two regions, the upper part of the chart, where $(t/\lambda)\,\mathrm{Im}[\mu] \geq 1$, the relationship is the same as previous charts can be defined as,

$$\mathrm{Re}[\varepsilon] = \mathrm{Re}[\mu] \tag{4.28}$$

$$\tan\delta_{\varepsilon} = \tan\delta_{\mu} \tag{4.29}$$

The lower region of the chart, where $(t/\lambda)\,\mathrm{Re}[\varepsilon] \leq 0.75$ while $(t/\lambda)\,\mathrm{Im}[\mu]$ changes, the same value of the $(t/\lambda)\,\mathrm{Re}[\mu]$ satisfies the Equation (4.27).

F. SUMMARY

In this chapter the main attention is given to matched wave impedance concept, in which the wave impedance at the front surface of the reflector backed material layer is made equal to the intrinsic impedance of free space to produce no reflection.

The material configuration and electromagnetic parameter values of a single homogeneous layer of dielectric/magnetic material to produce zero specular reflection has been determined for several backing materials.

The equations based on this concept are solved numerically using computer algorithms in order to plot universal design charts for zero specular reflection. Three different background layers are used for the charts: (1) perfect electric conductor, (2) free space, and (3) graphite. One can pick the required values from the charts for an ideal dielectric/magnetic layer. The extension can be made to any material to plot its zero specular reflection chart.

In the following chapter, numerical simulations of plates are performed to estimate the effectiveness of the layer in reducing RCS, and examine the sensitivity of performance to small change to the layer's constituent parameters.

THIS PAGE INTENTIONALLY LEFT BLANK

V. MODELING AND SIMULATION OF THE MATCHED WAVE IMPEDANCE THEORY

A. INTRODUCTION

In this chapter, the universal design charts, discussed in Chapter IV, are used to design radar absorbing material. Their effectiveness is evaluated using CST Microwave Studio program simulations. The platform's radar cross section is calculated with and without radar absorbing material, and the results are compared. The baseline for comparison is a rectangular plate with the dimensions shown in Figure 21.

B. PERFECT ELECTRIC CONDUCTOR

1. Model

In the first simulation, the backing material is a perfect electric conductor (PEC). Figure 16 is used to choose material properties and the thickness of the radar absorbing material. The PEC plate is 3 m by 2 m in the x and y directions. The frequency is 300 MHz and the wavelength is 1 m. The thickness of the plate in the z axis is 0.001 m.

The absorbing layer's electrical properties are chosen from Figure 16 as

$$\begin{aligned} &\tan\delta_{\varepsilon} = 0.3 \\ &t/\lambda\,\mathrm{Re}[\varepsilon] = 0.3 \\ &t/\lambda\,\mathrm{Re}[\mu] = 0.1103 \\ &t/\lambda\,\mathrm{Im}[\mu] = 0.1266. \end{aligned} \tag{6.1}$$

The magnetic loss tangent is calculated as

$$\tan\delta_{\mu} = \frac{t/\lambda\,\mathrm{Im}[\mu]}{t/\lambda\,\mathrm{Re}[\mu]} = \frac{0.1266}{0.1103} = 1.147. \tag{6.2}$$

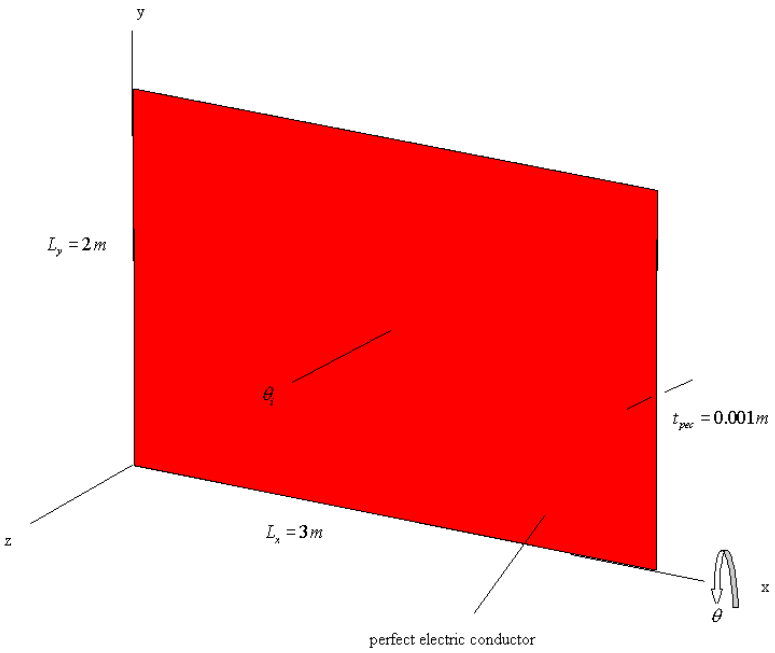

Layer type = PEC

Figure 21. Plate 1: Perfect Electric Conductor

The t/λ value is set to 0.1 so the required thickness for the absorbing material is 0.1 when the wavelength is 1 m. The real part of the permeability and permittivity of the coating material is calculated as

$$\begin{aligned} t/\lambda \,\mathrm{Re}[\varepsilon] &= 0.3 \\ t/\lambda \,\mathrm{Re}[\mu] &= 0.1103 \\ t/\lambda &= 0.1 \\ \mathrm{Re}[\varepsilon] &= 3 \\ \mathrm{Re}[\mu] &= 1. \end{aligned} \tag{6.3}$$

The radar absorbing material is designed using the relationships derived above, and the total thickness of the combined plate and the absorbing coating is 0.101 m. In Figure 22, the side cut of the model with radar absorbing material is seen with RAM

electrical properties listed in the corner. The red plate is PEC, and the blue plate is the radar absorbing material.

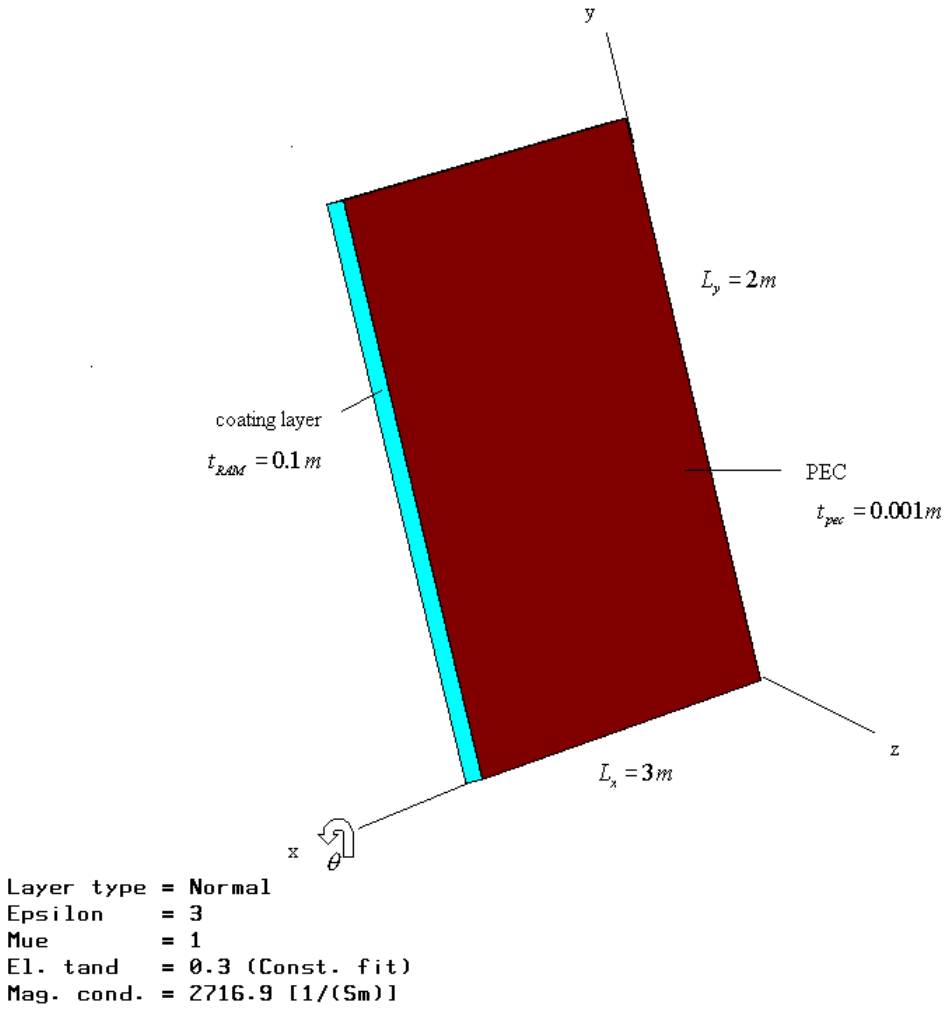

Figure 22. PEC plate with Radar Absorbing Material

2. Results

The simulations were run at 300 MHz and the plane wave incidence direction is in the $-z$ direction ($\theta_i = 0^o$ and $\phi_i = 90^o$) during the simulation process. The model is positioned at $\theta = 0^o$ and the bistatic RCS patterns of the model are collected by rotating the plate $0^o \le \theta \le 60^o$ in one degree increments. The required RCS value of interest is the monostatic (backscattered) value, which is used for the comparison. Figures 23 and 24

are bistatic RCS patterns of the model with and without radar absorbing material for $\theta = 0^o$.

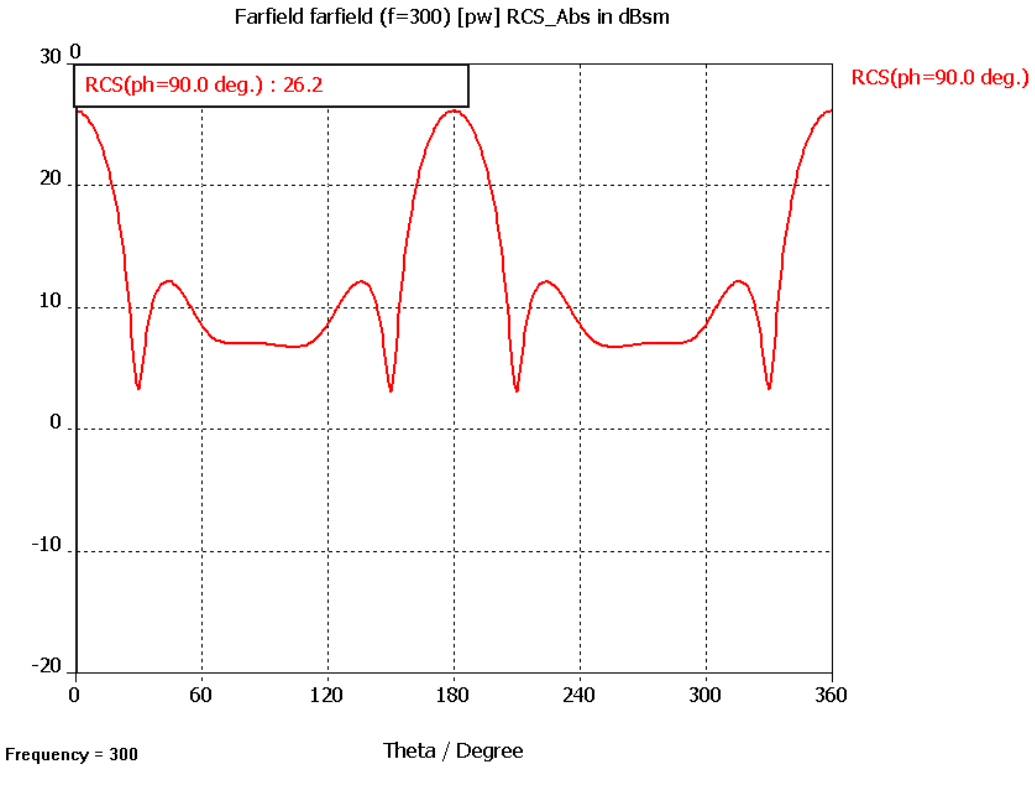

Figure 23. Bistatic RCS pattern of PEC plate without RAM for $\theta_i = 0^o$.

Figure 23 is the bistatic RCS pattern of PEC alone. The monostatic radar cross section value of the PEC is 26.2 dB for $\theta = 0^o$. This value is reduced to 3.841 dB with the RAM coating, which is shown in Figure 24. The reduction is approximately 23 dB.

In Figure 25, the total radar cross section pattern is plotted for $0^o \le \theta \le 60^o$ with and without radar absorbing material. In the main lobe, where θ is smaller than 17 degrees, and in the first lobe, where θ is smaller than 32 degrees, the reduction in the monostatic RCS is clearly seen. For larger angles the reduction decreases because the path length through the coating increases, so the thickness is no longer 0.1λ.

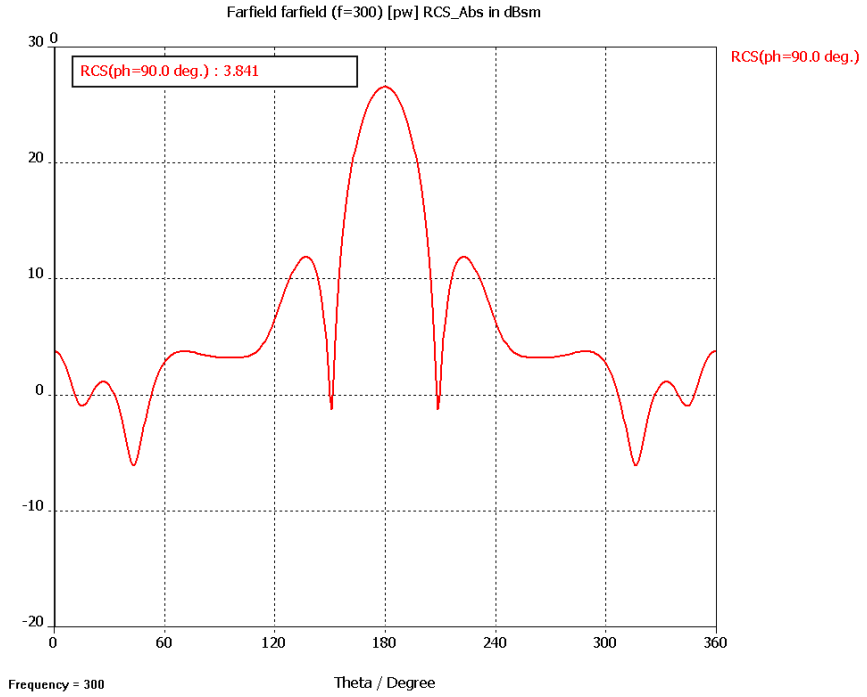

Figure 24. Bistatic RCS pattern of PEC plate with RAM for $\theta_i = 0^o$.

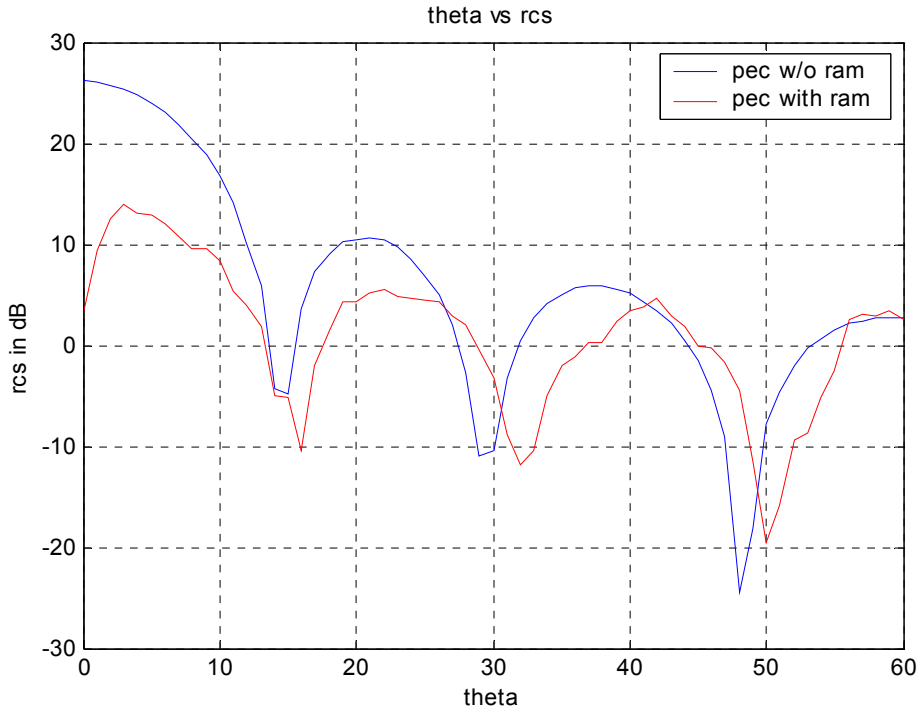

Figure 25. Monostatic RCS pattern of PEC plate with and without RAM.

Ideally the RCS at $\theta = 0^o$ should be $0\,\mathrm{m}^2$ (zero backscatter) if the four parameters are chosen exactly to satisfy the transcendental equation. In the numerical model, sources of error are:

1. the plate is not infinite, and edge diffraction is a source of RCS, and
2. numerical errors exist in the calculation of RCS.

The numerical errors are due to the lack of convergence and the approximation that arise from meshing the plate and RAM. This effect is illustrated in Figure 25 by the ripple in the sidelobes of the pattern. The sidelobe structures for the coated plate pattern should be smooth like the PEC sidelobe.

To estimate the sensitivity of the RAM parameters in determining RCS a tolerance study was done. The results are discussed in Section D.

C. GRAPHITE BACKING MATERIAL

1. Model

For the second simulation, the backing material is graphite. Figure 20 is used to choose material properties for the radar absorbing material. The graphite plate model is 3λ by 2λ as in the case of the PEC. The thickness of the model in the *z* direction is 0.02 m. The electrical properties of the graphite used in model design are

$$\begin{aligned} \varepsilon_r' &= 12 \\ \varepsilon_r'' &= 2.4 \\ \tan\delta_\varepsilon &= 0.2 \\ \tan\delta_\mu &= 0 \\ t_{graphite} &= 0.02\,\mathrm{m}. \end{aligned} \tag{6.4}$$

The absorbing layer's electrical properties are chosen from Figure 20 is as follows

$$\begin{aligned} &\tan\delta_{\varepsilon} = 0.3 \\ &t/\lambda\,\mathrm{Re}[\varepsilon] = 0.5 \\ &t/\lambda\,\mathrm{Re}[\mu] = 0.099 \\ &t/\lambda\,\mathrm{Im}[\mu] = 0.197. \end{aligned} \tag{6.4}$$

The magnetic loss tangent is calculated as

$$\tan\delta_{\mu} = \frac{t/\lambda\,\mathrm{Im}[\mu]}{t/\lambda\,\mathrm{Re}[\mu]} = \frac{0.099}{0.197} = 0.5025 \tag{6.5}$$

The t/λ value is set to be 0.197 so the required thickness for the absorbing material is 0.197 m where the wavelength is 1 m, and the real part of permeability and permittivity of the coating material are calculated as

$$\begin{aligned} &t/\lambda\,\mathrm{Re}[\varepsilon] = 0.3 \\ &t/\lambda\,\mathrm{Re}[\mu] = 0.197 \\ &t/\lambda = 0.197 \\ &\mathrm{Re}[\varepsilon] = 1.5228 \\ &\mathrm{Re}[\mu] = 1. \end{aligned} \tag{6.6}$$

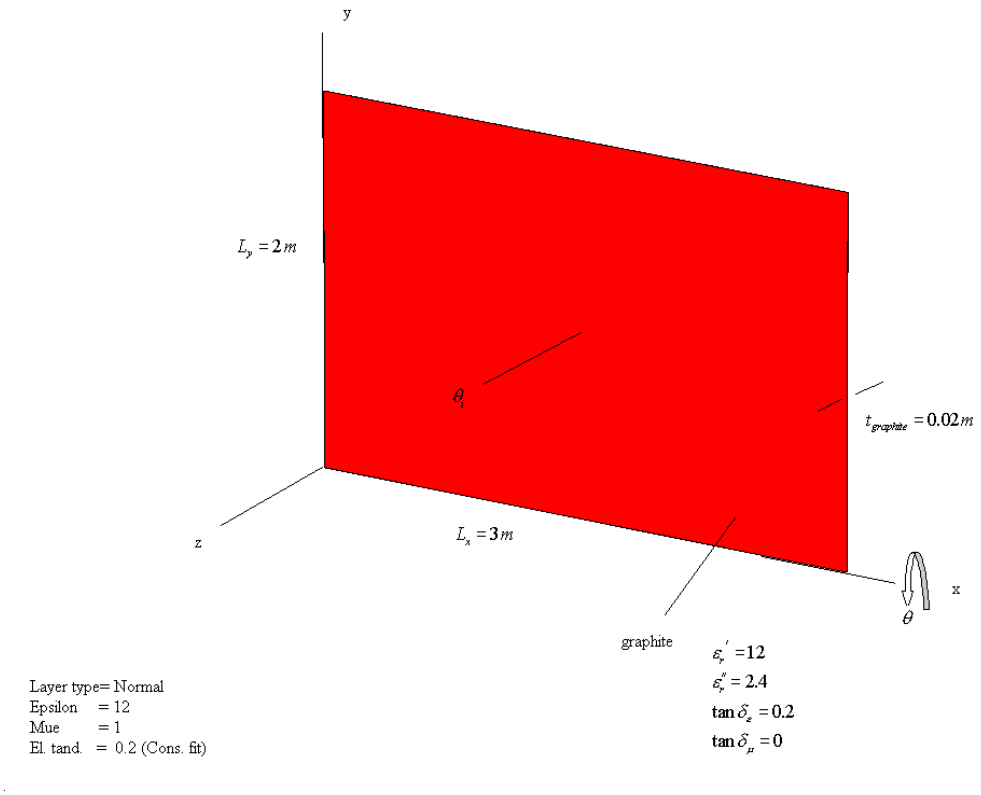

Figure 26. Plate 2 : Graphite.

The radar absorbing material is designed using the relationships derived above, and the thickness of the model with the absorbing coating is 0.217 m. In Figure 27, an oblique view of the model with radar absorbing material is seen, with RAM electrical properties listed in the corner. The red plate is the graphite, and the blue plate is the radar absorbing material.

2. Results

The simulations were run at 300 MHz with the plane wave incident from the –*z* direction ($\theta_i = 0^o$ and $\phi_i = 90^o$) during the simulation process. The model is positioned at $\theta = 0^o$ and the bistactic RCS patterns of the model are collected by rotating plate

$0^o \le \theta \le 60^o$ in one degree increments. The required RCS value of interest is the monostatic (backscattered) value, which is used for the comparison. Figures 28 and 29 are the bistatic RCS pattern of the graphite plate with and without radar absorbing material for $\theta = 0^o$.

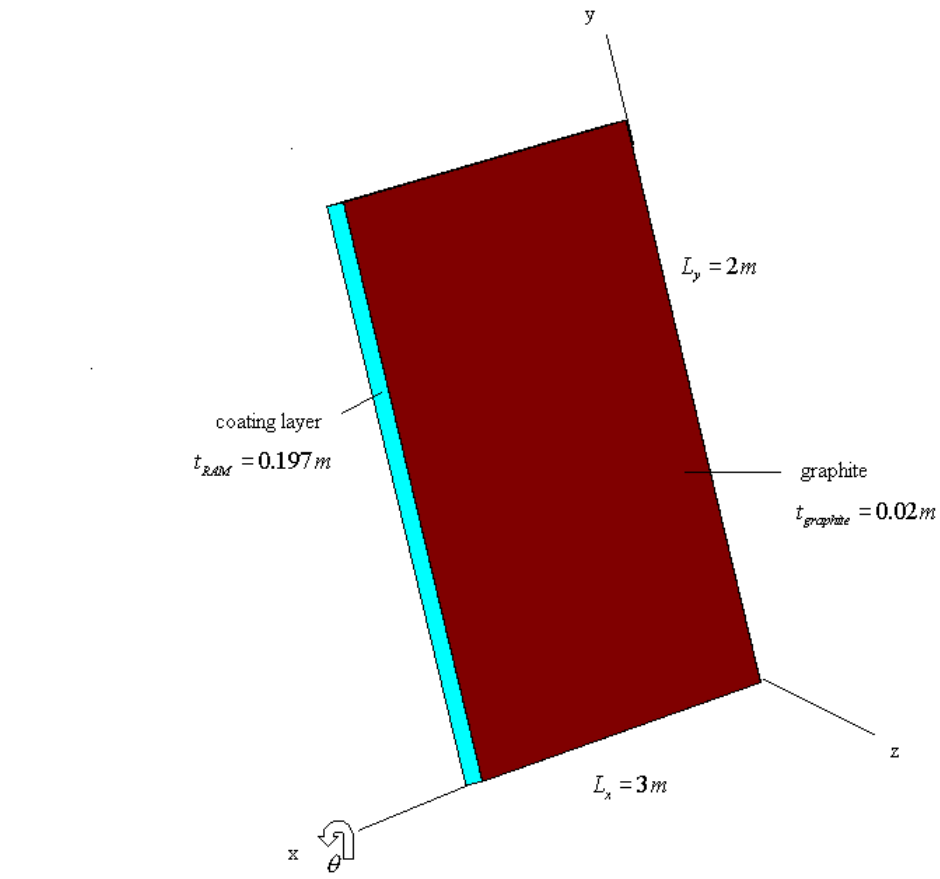

Figure 27. Graphite plate with Radar Absorbing Material.

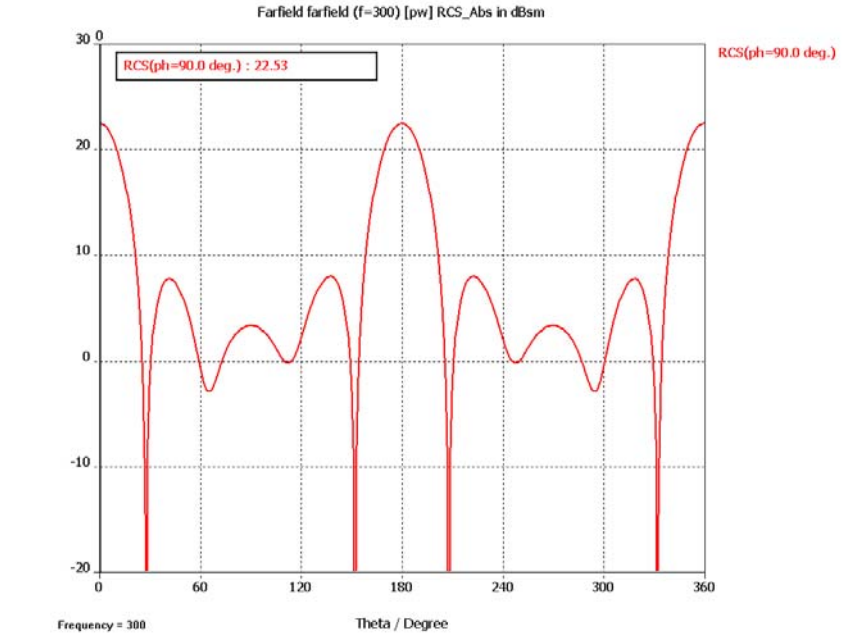

Figure 28. Bistatic RCS pattern of graphite plate without RAM for $\theta_i = 0^o$.

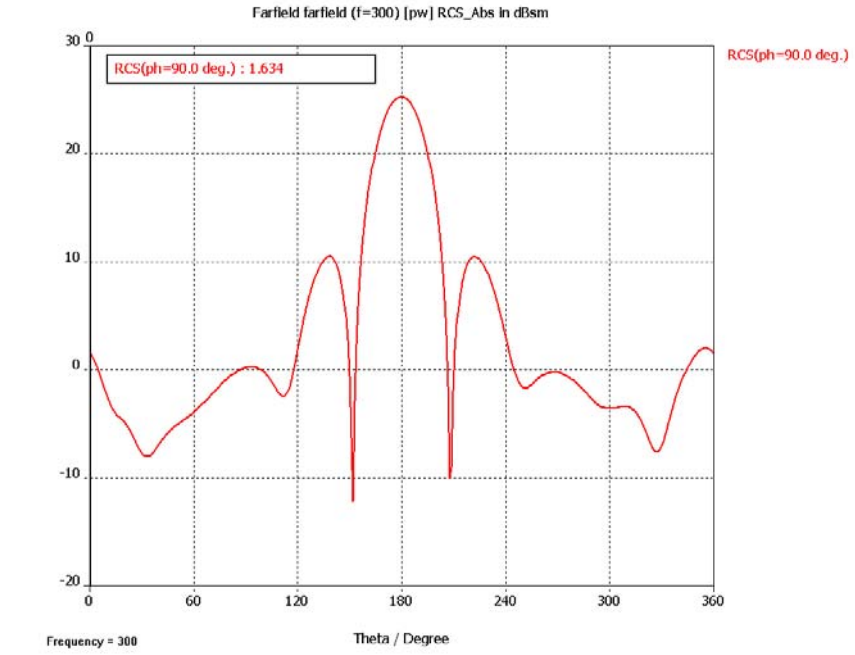

Figure 29. Bistatic RCS pattern of graphite plate with RAM for $\theta_i = 0^o$.

In Figure 28, the bistatic RCS pattern of the graphite plate is shown. The monostatic RCS value of the graphite background material is 22.53 dB. This value is reduced to 1.634 dB with the coated plate, which is shown in Figure 29, and the reduction is approximately 21 dB.

In Figure 30, the monostatic radar cross section pattern of the graphite plate model is plotted with and without radar absorbing material. For angles smaller than about 42 degrees, the reduction in the monostatic RCS is clearly seen. As in the case of the PEC coated plate, the RCS reduction is limited by edge diffraction and numerical errors.

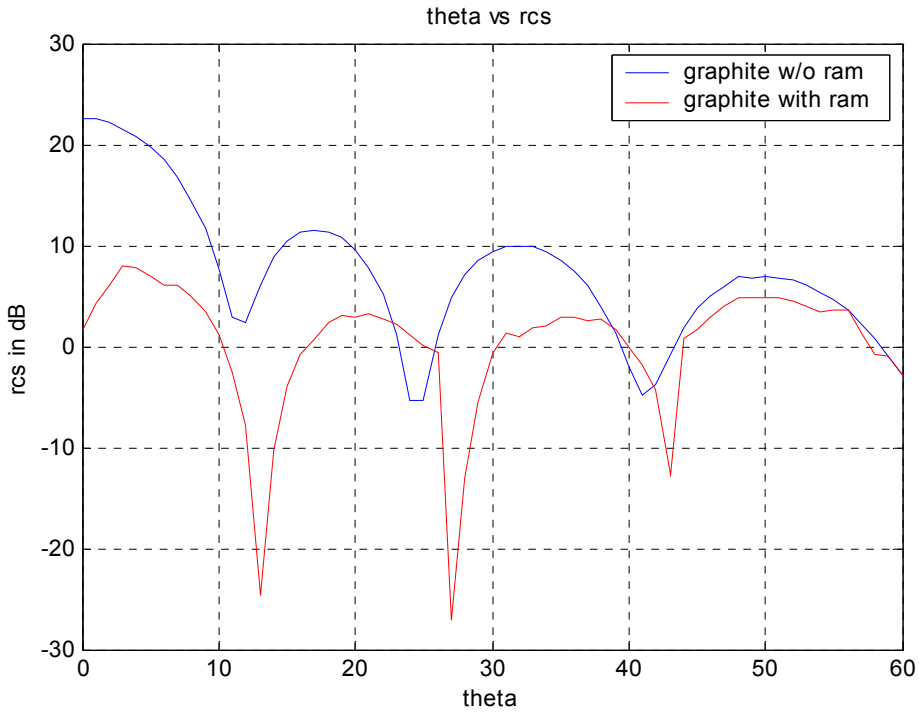

Figure 30. Monostatic RCS pattern of Graphite with and without RAM.

D. SENSITIVITY OF RCS TO CONSTITUTIVE PARAMETERS

In order to analyze sensitivity of the RCS to a change in one of the six parameters, the real part of dielectric constant is changed, $(1 \le \mathrm{Re}[\varepsilon] \le 4.5)$ and then the RCS of the coated plate is recalculated. The results are shown in Figure 31.

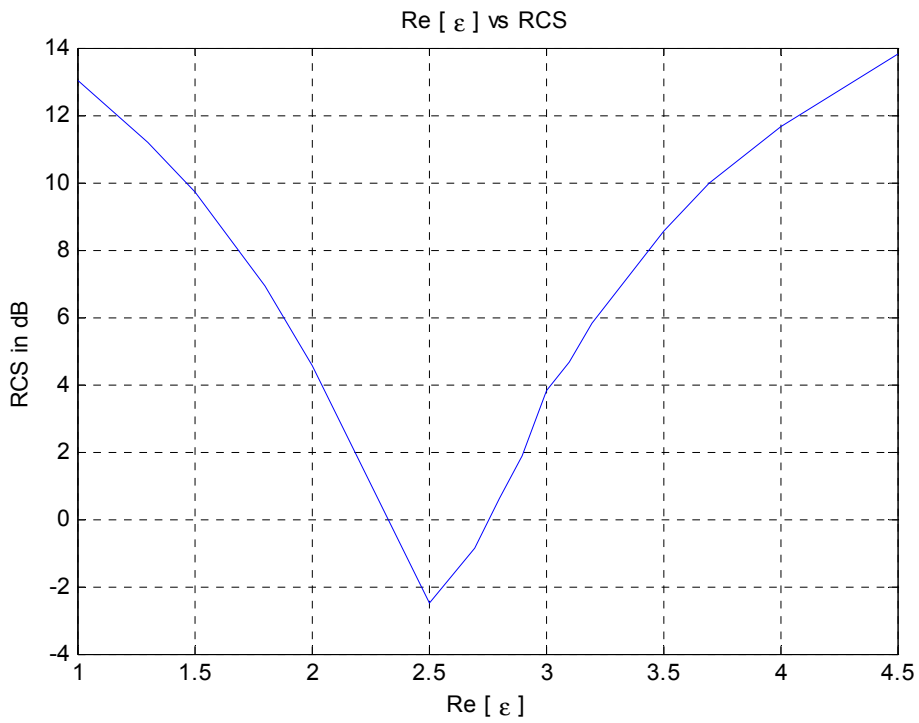

Figure 31. Sensitivity of RCS versus ε_r'

The coated plate RCS results presented in Section B were done with $\mathrm{Re}[\varepsilon] = 3$. The change in the RCS results close to this value is not large. From Figure 31 it is seen that $\varepsilon_r' \approx 2.5$ actually gives more reduction. The reason is that edge diffraction exists for a finite plate and the RAM parameters assume an infinite plate. To achieve minimum RCS for a finite plate it is necessary to "detune" the absorber so that it reflects enough to cancel the diffracted field.

In summary, it appears that the RAM performance is not overly sensitive to the parameter values, at least not for the upper right-hand area of the chart.

E. SUMMARY

In this chapter the results of two RAM plate models were presented. (1) perfect electric conductor, and (2) graphite. The reduction in monostatic radar cross section value is clearly seen near normal incidence and in the first few lobes compared to uncoated plates.

The first step in the design process is to pick the permeability and permittivity values precisely from the universal design charts in order to obtain effective radar cross section reduction. Depending on the frequency of interest, one should choose the related material properties to have a small thickness to wavelength ratio in order to cut down the additional total weight of the coated plate.

THIS PAGE INTENTIONALLY LEFT BLANK

VI. CONCLUSIONS

The importance of radar cross section reduction was discussed, and the major RCSR techniques summarized. Low observable platforms have extremely low RCS specifications that cannot be achieved by shaping alone. The application of RAM is necessary, in which case the appropriate constitutive parameters and thickness must be selected. The universal design chart gives combinations of μ, ε and t that provide zero specular reflection at normal incidence.

Three different backing materials were used to generate the charts: (1) perfect electric conductor, (2) free space, and (3) graphite. One can pick the required values from the charts for an ideal zero reflection dielectric/magnetic layer. The extension to other materials is straightforward.

Numerical simulations of coated plates were performed to estimate the effectiveness of the absorbing layers in reducing RCS. The reduction in monostatic radar cross section value is shown by plotting the radar cross section of the plate with and without radar absorbing material. In the design process, permeability and permittivity values should be picked precisely from the universal design charts in order to obtain effective radar cross section reduction. The thickness to wavelength ratio is important, since it is based on the frequency at which threat radar is going to operate. One should choose the required material properties so as to obtain a thin layer in order to cut down the additional weight. Of course the selected complex μ_r and ε_r must be physically realizable.

The effectiveness of the matched surface RAM technique depends on the accuracy of the dielectric/magnetic values that are picked off from the charts. A limited tolerance study for one set of parameters indicated that changes in ε of 5% did not significantly affect the RCS reduction. It is expected that the sensitivity of the reduction to small changes in μ and ε would be greatest for the area of the chart where $\mu_r \approx \varepsilon_r$. The numerical radar cross section calculations performed based on these values verified the effectiveness of the absorbing layer.

There are several topics that should be investigated in future research. One is to examine the behavior of the layer for off normal incidence angles, and see whether there are any ways to reduce the sensitivity to angle. A second potential area of research is to continue the plate simulations to determine RCSR tolerance to small changes in μ_r and ε_r. When the materials are manufactured they can only be specified within a range; for example, $\varepsilon_r' = 3.0$ would be provided from the manufacturer as 3.0 ± 0.05.

Finally, it should be possible to extend the transcendental equation solution to multiple layers. They should be able to provide wide frequency and angle regions. However, the number of parameters will double and it is not clear how to present all of the parameter space on a single chart.

LIST OF REFERENCES

1. Eugene F. Knott, John F. Schaeffer, Michael T. Tuley, *Radar Cross Section*, 2nd edition, Artech House, 1993.
2. David C. Jenn, *Radar and Laser Cross Section Engineering*, AIAA, 1995.
3. Federation of American Scientist Official Website (www.fas.org), 22 June 2003.
4. Asoke Bhattacharyya, D.L. Sengupta, *Radar Cross Section Analysis & Control*, Artech House, 1991.
5. V. H. Weston, "Theory of Absorbers in Scattering," *IEEE Transactions on Antennas and Propagation*, Vol. AP, No. 4, September 1963.
6. Geoge T. Ruck, Donald E. Barrick, William D. Stuart, Calerence K. Krichbaum, *Radar Cross Section Handbook*, 2nd edition, 1970.
7. H. M. Musal, Jr., D. C. Smith, "Universal Design Chart for Specular Absorbers," *IEEE Transactions on Magnetics*, Vol. 26, No. 5, September 1990.
8. B. C. Hoskin, A. A. Baker, *Composite Materials for Aircraft Structures*, AIAA, 1986.
9. M. Dresselhaus, G. Dresselhaus, K. Sugihara, I. Spain, H. A. Goldberg *Graphite Fibers and Filaments*, Springer-Verlag Berlin Heidelberg, 1988.
10. Fawwaz T. Ulaby, *Fundamentals of Applied Electromagnetics*, Media Edition, Prentice Hall, 2001.

THIS PAGE INTENTIONALLY LEFT BLANK

INITIAL DISTRIBUTION LIST

1. Defense Technical Information Center
   Ft. Belvoir, Virginia

2. Dudley Knox Library
   Naval Postgraduate School
   Monterey, California

3. Chairman
   Information Sciences Department
   Monterey, CA

4. Professor David C. Jenn
   Department of Electrical and Computer Engineering
   Monterey, CA

5. Professor Richard D. Adler
   Department of Electrical and Computer Engineering
   Monterey, CA

6. 1LT. Cihangir Kemal Yuzcelik
   Turkish Airforce
   Turkey

7. Hava Harp Okulu
   Hava Harp Okulu Kutuphanesi
   Yesilyurt, Istanbul

8. Deniz Harp Okulu
   Deniz Harp Okulu Kutuphanesi
   Tuzla, Istanbul

9. Kara Harp Okulu
   Kara Harp Okulu Kutuphanesi
   Bakanliklar, Ankara